

© 2017

Jonathan Elliot Holzsager

ALL RIGHTS RESERVED

THE EFFECTS OF COAXIAL PROPELLERS FOR THE  
PROPULSION OF MULTIROTOR SYSTEMS

By

JONATHAN ELLIOT HOLZSAGER

A thesis submitted to the  
Graduate School of New Brunswick  
Rutgers, The State University of New Jersey

In partial fulfillment of the requirements

For the degree of

Master of Science

Graduate Program in Mechanical and Aerospace Engineering

Written under the direction of

Professor Francisco Javier Diez-Garias

And approved by

---

---

---

New Brunswick, New Jersey

October 2017

## **ABSTRACT OF THE THESIS**

### **The Effects of Coaxial Propellers for the Propulsion of Multirotor Systems**

**By JONATHAN ELLIOT HOLZSAGER**

**Thesis Director:**

**Professor Francisco Javier Diez-Garias**

**Multirotor vehicles offer access to the skies for users across all walks of life and industry due to their simplicity, availability, and low cost. Although advancements continue, developers are slowed by the limits of available propulsion systems. Coaxial rotors stack propellers over one another to provide more thrust without increasing a vehicle's footprint nor battery voltage. Previous investigations studied the thrust lost to coaxial rotor systems, wherein downstream propellers produced less thrust than their predecessors. This experimental study examines the effects of propeller spin direction, separation distance, motor speed, and propeller pitch to explore different methods of recuperating thrust losses. During testing, each propeller's thrust, current draw, and rotational speed was measured. Results show that for 13-inch propellers, reducing the distance between the planes of rotation from 8 to 2 inches produced variations up to 123 grams of thrust, representing a 4.5% improvement. Controlling the motors' speeds independently confirmed that a coaxial pair will provide thrust most efficiently if the back (downstream) motor is operated at a higher throttle setting than the front (upstream) motor. Similarly, a coaxial pair will provide more thrust if the back propeller's pitch is higher than the front propeller's pitch. This was applied to the effect that the back propeller in a coaxial pair provided 119% of the thrust of the front propeller. This allowed for a coaxial pair's thrust to range between 1790 and 2530 grams, allowing for a 41% increase in thrust from the worst case to the best case. When varying propeller pitch was applied to six different arrangements of four propellers, maximum thrusts ranged between 2960 and 4010 grams. One of these coaxial quadruplets was tested to provide a total of 401% of the thrust of its front propeller.**

## Table of Contents

<b>Abstract</b> .....	ii
<b>Table of Contents</b> .....	iii
<b>Table of Tables</b> .....	iv
<b>List of Figures</b> .....	v
<b>1.Introduction</b> .....	1
<b>1.1 Literature Review</b> .....	4
<b>1.2 Theory</b> .....	8
<b>2.Experimental Setup</b> .....	12
<b>2.1 Equipment Details</b> .....	12
<b>2.2 Calibration</b> .....	15
<b>2.3 Experimental Procedure</b> .....	16
<b>2.4 System Diagrams</b> .....	16
<b>2.5 Uncertainty in Measurement Equipment</b> .....	18
<b>2.6 Considering Vibrations</b> .....	19
<b>3.Results</b> .....	20
<b>3.1 Four Coaxial Propellers</b> .....	20
<b>3.2 Two Coaxial Propellers of Different Speeds</b> .....	29
<b>3.3 Two Coaxial Propellers of Different Pitches</b> .....	41
<b>3.4 Four Coaxial Contra-rotating Propellers of Different Pitches</b> .....	44
<b>4.Conclusions</b> .....	49
<b>4.1 Future Experiments</b> .....	50
<b>References</b> .....	51

## Table of Tables

<b>Table 1.</b> Six different propellers used in experiments .....	15
<b>Table 2.</b> Test matrix summarizes the spin directions of the rotors. ....	20

## Table of Equations

{Equation 1} <i>advance ratio: <math>J</math></i>	8
{Equation 2} <i>thrust: <math>T</math></i>	9
{Equation 3} <i>torque: <math>Q</math></i>	9
{Equation 4} <i>mechanical poer: <math>P_{out}</math></i>	9
{Equation 5} <i>mechanical power: <math>P_{out}</math></i>	9
{Equation 6} <i>electrical power: <math>P_{in}</math></i>	9
{Equation 7} <i>efficiency: <math>\eta</math></i>	9
{Equation 8} <i>performance: <math>\Pi</math></i>	10
{Equation 9} <i>blade element thrust (<math>u = 0</math>): <math>T_1</math></i>	10
{Equation 10} <i>blade element torque (<math>u = 0</math>): <math>Q_1</math></i>	10
{Equation 11} <i>blade element thrust (<math>u &gt; 0</math>): <math>T_2</math></i>	11
{Equation 12} <i>blade element torque (<math>u &gt; 0</math>): <math>Q_2</math></i>	11

## List of Figures

<b>Figure 1.</b> Breguet-Richet's Gyroplane No.1 .....	1
<b>Figure 2.</b> The Swarm electric passenger multirotor aerial vehicle.....	2
<b>Figure 3.</b> The Naviator unmanned multi-medium vehicle (UMMV).....	3
<b>Figure 4.</b> Flow diagram of a single rotor and a coaxial rotor pair.....	4
<b>Figure 5.</b> Performance trends for air propellers plots .....	8
<b>Figure 6.</b> Reduction of angle of attack for propeller blade section .....	10
<b>Figure 7.</b> Photograph of test equipment during experiment.....	12
<b>Figure 8.</b> Pitch of a propeller, illustrated .....	14
<b>Figure 9.</b> Propeller arrangement and simplified diagram.....	16
<b>Figure 10.</b> Diagram of test equipment connections, 4 rotors. ....	17
<b>Figure 11.</b> Diagram of test equipment connections, 2 rotors .....	17
<b>Figure 12.</b> Diagram of test equipment connections, 2 individually-controlled rotors .....	18
<b>Figure 13.</b> Thrust of three trials of contra-rotating coaxial quadruplet.....	21
<b>Figure 14.</b> Thrust of three trials of co-rotating coaxial quadruplet .....	22
<b>Figure 15.</b> Simplified diagrams of coaxial and multi-axis propeller configurations.....	23
<b>Figure 16.</b> Total thrust of coaxial and multi-axis systems .....	23
<b>Figure 17.</b> Coaxial to multi-axis total thrust ratios .....	24
<b>Figure 18.</b> Thrust of co-rotating coaxial quadruplet with higher pitch .....	25
<b>Figure 19.</b> Performance reduces with each additional rotor.....	26
<b>Figure 20.</b> Mechanical and electrical power compared for coaxial and multi-axis system .....	27
<b>Figure 21.</b> Thrust of contra-rotating coaxial quadruplet at varying distances.....	27
<b>Figure 22.</b> Total thrust versus current for different separation distances .....	28
<b>Figure 23.</b> Performance versus number of rotors.....	29

<b>Figure 24.</b> Effect of front motor speed on back motor speed.....	30
<b>Figure 25.</b> Effect of front motor speed on front rotor thrust .....	31
<b>Figure 26.</b> Effect of front motor speed on back rotor thrust .....	32
<b>Figure 27.</b> Effect of front motor speed on total thrust of coaxial pair.....	33
<b>Figure 28.</b> Effect of front motor speed on front motor current. ....	34
<b>Figure 29.</b> Effect of front motor speed on back motor current. ....	35
<b>Figure 30.</b> Effect of front motor speed on total current of coaxial pair. ....	36
<b>Figure 31.</b> Total thrust versus total current for coaxial pair.....	37
<b>Figure 32.</b> System efficiency versus total thrust for coaxial pair.....	38
<b>Figure 33.</b> Heat map of total thrust for combinations of throttle settings .....	39
<b>Figure 34.</b> Heat map of system efficiency for combinations of throttle settings .....	40
<b>Figure 35.</b> Effect of front motor speed on system performance.....	40
<b>Figure 36.</b> Heat maps of total thrust for combinations of co-rotating pitches.....	41
<b>Figure 37.</b> Heat maps of total thrust for combinations of contra-rotating pitches .....	42
<b>Figure 38.</b> Heat maps of back-to-front thrust ratio for co-rotating pitches .....	43
<b>Figure 39.</b> Heat maps of back-to-front thrust ratio for contra-rotating pitches .....	43
<b>Figure 40.</b> Heat maps of system efficiency for contra-rotating pitches .....	44
<b>Figure 41.</b> Thrust distribution of 4L-6.5R-8L-10R quadruplet.....	45
<b>Figure 42.</b> Thrust curves for six coaxial quadruplets.....	46
<b>Figure 43.</b> Efficiency curves for six coaxial quadruplets.....	46
<b>Figure 44.</b> Performance curves for six coaxial quadruplets .....	47
<b>Figure 45.</b> Maximum current of the quadruplets is directly related to the collective pitch .....	48

## 1. Introduction

Multicopter vehicles have their origins in the early 1900s with the Breguet-Richet Gyroplane No.1, shown in Figure 1 below. This experimental quadrotor was powered by a 36.7-kilowatt engine and controlled by a pilot who could only control engine throttle. Due to stability issues, its designers abandoned the multicopter form for helicopters and fixed-wing aircraft.<sup>1</sup> However, these vehicles have recently experienced a renaissance due to the introduction of small on-board computers that can precisely control individual electric motors' speeds. This technology makes multicopter vehicles highly controllable, such that they can achieve movement with six degrees of freedom.<sup>2</sup> They continue to be increasingly prevalent, finding use in scientific data collection<sup>3</sup>, recreational photography<sup>1</sup>, and infrastructural surveys<sup>2</sup> to name a few. However, sectors such as transportation also demonstrate the desire to apply this technology. On the smaller scale, companies such as Amazon have proposed autonomous package delivery.<sup>4</sup> On the larger scale, companies and individuals are taking strides to introduce electric passenger multicopter aerial vehicles. According to conservative estimates, autonomous aerial passenger and cargo transport may be popularly accepted by 2035.<sup>5</sup>

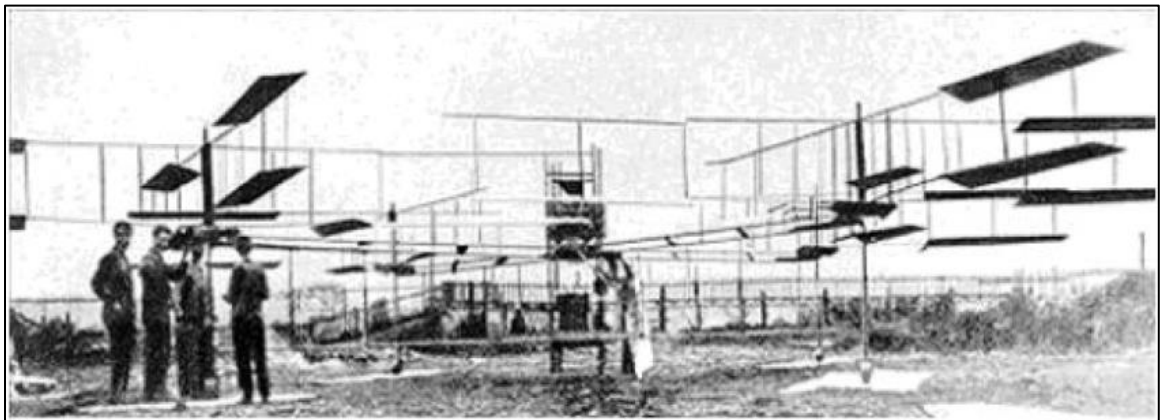


**Figure 1.** Breguet-Richet's Gyroplane No.1 enabled vertical flight using a multicopter setup as early as 1907.<sup>1</sup>

In order to operate multicopter systems with passenger and cargo transport capabilities, some issues need to be addressed: low payload capacity, low vehicle endurance, and low resilience to crosswinds.<sup>2</sup> In an effort to overcome these concerns, engineers continue to develop novel variations on the standard quadrotor form. For instance, researchers constantly work on increasing the total thrust of the propulsion systems. However, engineers are already running into the limitations of commercially available products. For

specialized larger projects, they will have to enter into manufacturing custom parts such as specially designed motors and propellers. This can be cost-prohibitive and delay the progress of the state of the art.

While using the motors and propellers already available to them, engineers can still increase a vehicle's thrust by including more motors and propellers. One of the benefits of this is that the same voltage can be used to drive the system instead of advancing to potentially dangerously high voltages. Instead, battery capacities can be increased to accommodate the higher number of propellers. If this is done, a developer must determine where to position the additional propellers relative to each other.

One option is to expand the propulsion system horizontally outward. This is a popular approach among backyard engineers interested in personal electric aerial vehicles, as illustrated in Figure 2. The vehicle shown incorporates 54 closely packed propellers to successfully lift its passenger, but it occupies a platform area about seven times that of the passenger. Although this approach is feasible, continuously increasing the footprint of the vehicle is eschewing the fact that in a practical setting, the vehicle's size might be limited to the space of a helipad or the width of a passage such as a tunnel or door.



**Figure 2.** YouTube user gasturbine101's The Swarm is a proof-of-concept electric passenger multirotor aerial vehicle.

With limits on the widths of heavy payload multirotor systems, the natural progression in adding propellers is to expand the propulsion system vertically. This will provide additional thrust without increasing the vehicle's area it occupies on the ground. By stacking the motors, designers also make better use of the

vehicle's pre-existing structure, requiring no additional arms to support the next set of motors. This coaxial arrangement of propellers is already in popular use and is implemented on The Naviator, an unmanned multi-medium vehicle featured in Figure 3. This vehicle utilizes two planes of four propellers wherein the lower set is directly below the upper set. On each arm, two motors are mounted and motors rotate around a common axis, exemplifying a coaxial pair.

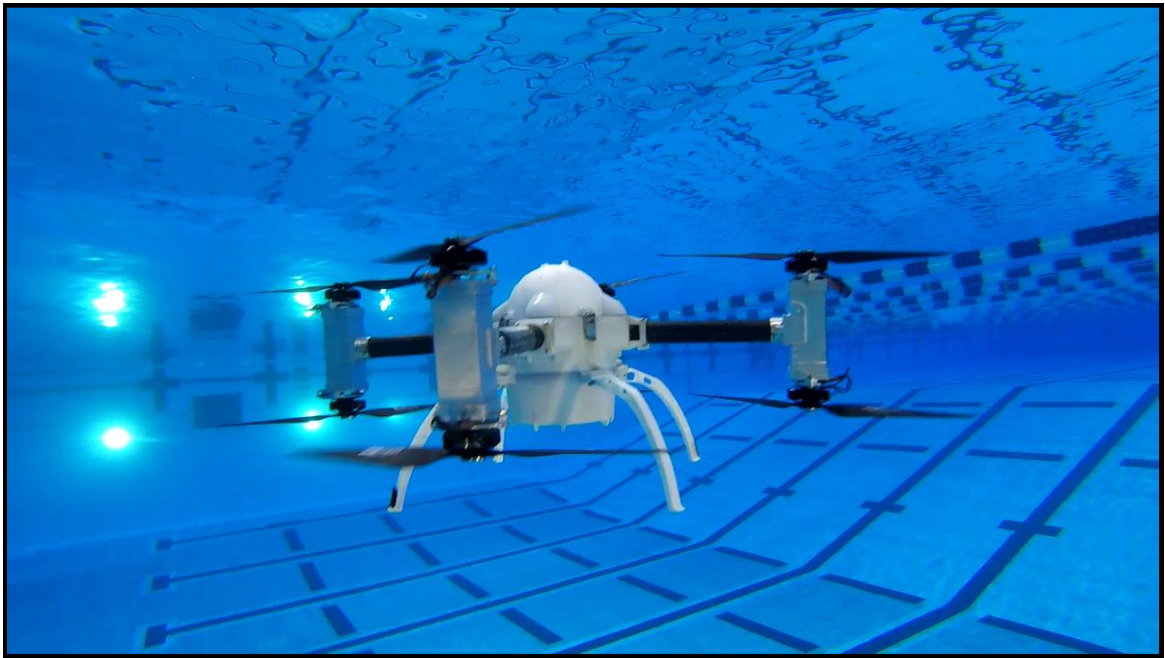


**Figure 3.** The Naviator is an unmanned multi-medium vehicle (UMMV) developed at Rutgers University.

In this form, quadcopter behavior still applies. For each plane of propellers, speeds can increase together to generate more thrust. Slowing propellers on the front or back result in pitching motion. Slowing propellers on the left or right result in rolling motion. Slowing diagonal sets of propellers create a torque imbalance that results in yaw. By setting the attitude (pitch, roll, and yaw) and varying the thrust of the system, the vehicle achieves control of its position.<sup>1</sup>

Coaxial propeller applications are limited to two tiers typically. The objective of the present research is to evaluate the potential of two or more coaxial propellers in terms of increasing the total thrust of the system based on experimental data.

## 1.1 Literature Review

Coaxial rotors systems have been under development since the first coaxial helicopter patent was awarded to Henry Bright in 1859<sup>6</sup>. Since then, many iterations of the coaxial helicopter have been designed, constructed, and used in civilian and military applications. According to a summary of coaxial rotor aerodynamic research by Coleman<sup>6</sup>, theoretical and experimental research across decades and nations have studied the aerodynamic effects of the coaxial setup on the performance of these helicopters. This survey addressed rotor separation distance, load sharing between rotors, wake structure, and swirl recovery amongst other studies.

Coleman included Taylor's 1950 work performing balsa dust flow visualizations on coaxial rotors, wherein it was observed that each rotor's wake remained separate in the flow<sup>7</sup>. Taylor's photographs showed that the lower rotor draws air from beyond the width of the upper rotor and from the flow of the upper rotor, as illustrated in Figure 4. This illustration is a simplified diagram of the control volumes of a single rotor and a coaxial rotor, along with scaled arrows to indicate magnitude and direction of the rotors' thrust and air flow. Upon inspection, the lower coaxial rotor produces a faster wake and less force than either the single rotor or its upper coaxial counterpart. This thrust loss is a reflection of wake interference that is inherent to coaxial rotor setups.<sup>6</sup> Comparative studies performed by the United Aircraft Research Laboratories in 1965 attributed the lesser thrust generated by the lower rotor to the downwash of the upper rotor<sup>6</sup>.

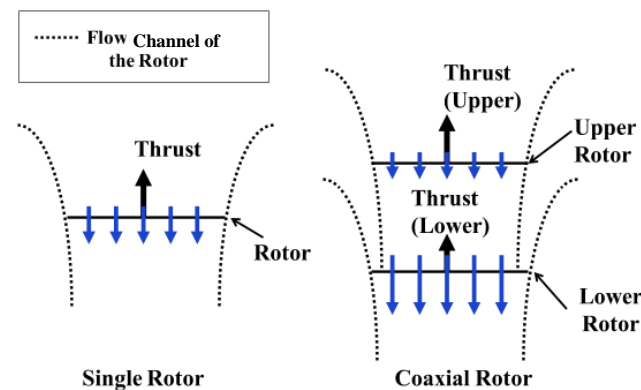


**Figure 4.** Flow diagram of a single rotor and a coaxial rotor pair. Arrow lengths are indicative of relative air speeds and thrust magnitudes.<sup>2</sup>

In 1985, Zimmer<sup>8</sup> performed aerodynamic calculations on coaxial rotors, noting an 11% propulsive advantage to a contra-rotating coaxial pair over a single rotor. Zimmer attributed this boon to the swirl recovery potential of opposite-rotating propellers. As Min pointed out in a study of contra-rotating propellers

in marine applications, a contradiction exists: swirl recovery dictates that propellers' planes of rotation should be as close as possible, yet the downstream propeller would also produce more thrust if the high pressure behind the upstream propeller could dissipate over a longer distance<sup>9</sup>. Such competing design principles necessitate optimization by experimentation and simulation.

Leishman and Ananthan<sup>10</sup> used momentum theory, finite volume method (FVM), and blade element momentum theory (BEMT) to characterize the flow of a coaxial rotor. Their models were then used to guide the design of an optimized coaxial rotor for hovering and axial flight. Rand and Khromov<sup>11</sup> also developed an aerodynamic optimization study for generic coaxial rotors in these flight modes with a focus on BEMT and a nonlinear characterization of rotors' downwash. Yana and Rand<sup>12</sup> integrated analytical, free wake, and rigid wake models into the optimization and found lower precision in the rigid wake model for system analysis and prediction. Xu and Ye<sup>13</sup> used computer models of coaxial rotors to observe the positive correlation between pitch and thrust and they found that as rotor plane separation distance increases, the lower rotor's coefficient of thrust decreases more than the upper rotor's coefficient of thrust increases.

Coaxial rotorcraft have also been the subject of acoustic research and the correlations between rotor design, wake geometry, and noise<sup>14</sup>. Kim et al<sup>15</sup> observed coaxial rotors to be 20-35 decibels noisier than a single rotor. Periodic studies such as these have also elucidated that upper and lower rotor thrust values increase as the blades approach and decrease after they overlap<sup>16</sup>. A study by Barbely et al<sup>17</sup> performed a simulation of passing blades and similar observations were made.

Lim et al<sup>18</sup> related the experimental performance of full-scale helicopter coaxial rotors and model-scale coaxial rotors. They noted that with a separation distance greater than 20% of the rotor diameter, the effect of spacing was minimal. Also, the team quantified thrust loss in the coaxial system. The lower rotor kept 81% of the thrust of a single motor (correcting for ground effect) while the upper rotor retained 90% of the thrust of a single motor. While this paper made strides in scaling down the rotors, its lessons cannot be fully extended to multirotor propellers, which more closely resemble the propellers of a model airplane than those of a model helicopters. This is because helicopter blades have a variable pitch while multirotor blades have a fixed pitch.

Brandt and Selig<sup>19</sup> recognized the need for propeller data suited to the miniature scale suited to the proliferating unmanned aerial vehicles (UAVs). They tested 79 propellers across various sizes (diameters

between 9 and 11 inches) and manufacturers in a wind tunnel. Calculated efficiencies varied between 28% and 65%, highlighting the importance of proper propeller selection for multirotor UAVs because the disadvantage of improper propeller selection can be multiplied tremendously. Testing performed by Merchant<sup>20</sup> preceded Brandt and Selig's work, but covered 31 propellers ranging in material (wood, glass fiber composite, carbon fiber composite), diameter (6 to 22 inches) and even used a three-bladed propeller.

Within the realm of quadcopter vehicles (not coaxial), rotor interactions have been studied. Intaratep et al<sup>21</sup> experimentally studied the acoustic signature of a DJI Phantom II but also made some thrust-related observations. They noted that two rotors produced 5.8% less thrust than expected and four rotors produced 7.3% less thrust than expected, based on multiplying the thrust of a single rotor. The interaction of rotors in a shared plane of rotation (as in the case of quadcopters) was analyzed computationally by Yoon et al<sup>22</sup>. They studied the aerodynamic interaction of the rotors, the fuselage, and the rotor arms (wings for a tilt-rotor). The addition of the fuselage to the simulation improved rotor efficiency by limiting interaction. On the other hand, a reduction in space between the rotors would decrease rotor efficiency.

Aleksandrov and Penkov<sup>23</sup> also looked at the form of small quadcopters. Their experiments used propellers with 8-inch and 10-inch diameters and 4.5-inch pitches in a simulation of a quadcopter. They varied the gap size between propellers in the same plane, as well as the motor speed, finding an optimal gap between adjacent propellers' tips to be 32.5 mm. For their vehicle, losses in thrust were more significant when the propellers were too close than when they were too far apart.

The domain of multirotor vehicles also includes tandem helicopters, in which the rotor blades overlap. The rotors are rotating on separate, parallel planes and the axes of rotation are closer than the blades' diameter. Shahmiri<sup>24,25</sup> performed tests in a subsonic wind tunnel and found that the system was most efficient when there was no overlap at low loadings. They<sup>26</sup> observed that with an overlap, power demand increased and that with overlap, best results occurred when the inter-planar distance was low and the area of overlap between 10% and 15% of the rotor disc area. However, his coaxial (100% overlap) tests supported larger separation distances between the propeller planes. They also experimented with different rotor support arms and found that the rotors are more efficient when interacting with a smaller arm, even if it is not a more aerodynamic shape. The importance of support arm shape was also stressed by Yoon<sup>22</sup>, who noted the wings of the tilt-rotor encounter drag from the rotors that result in a downward force on the vehicle.

Brazinskas<sup>27</sup> experimented with a pair of propellers with inter-planar separations between 5% and 85% of the rotor's diameter. He noted a 4% increase in system efficiency for a contra-rotating coaxial rotor over the efficiency of a co-rotating coaxial rotor. For a tandem system in which rotors did not rotate around a shared axis, peak efficiency was observed when the inter-planar separation was 5% of the rotor diameter and the inter-axial separation was 97% of the rotor diameter. This system was about 3% less efficient than two isolated propellers.

Otsuka and Nagatani<sup>2</sup> compared coaxial and tandem systems by rotating one quadcopter below another. They determined that when the rotor shafts are rotated around the vehicle's center by 45 degrees, two tiers of four propellers could generate approximately 90% of the thrust of eight independent propellers, as opposed to the 70% that corresponds to a zero degree rotation, a coaxial setup. This supports the consensus that rotor overlap is detrimental established by aforementioned sources.

Prior et al<sup>28</sup> decided to use a contra-rotating coaxial setup for their tri-rotor UAV due to the fact that each coaxial pair would balance its own rotor torque. Prior and Bell<sup>29</sup> noted the disagreements in the community regarding the dimensionless inter-planar rotor separation distance and attributed it to viscous losses at low Reynolds Numbers, the domain of many UAV rotors. Small-scale coaxial rotors were separated by an average distance of 31.5% of their diameters, while large-scale coaxial rotors were separated 9%.

Ducting multirotor propellers has also been researched. Lee<sup>30</sup> determined that the duct does not consistently improve the operation of the coaxial rotor in hover and forward flight, as it would for a single propeller. He commented that positioning the upper rotor close to the inlet was more beneficial than altering inter-planar rotor separation distance. Geldenhuys<sup>31</sup> applied Lee's results to guide his shrouded contra-rotating rotor design. Using six different meshes, he created a design that provides 24% more thrust than his initial design. That design was calculated to provide 80% more thrust than Lee's experiment at the same power input.

The existing studies concern themselves with identifying the losses due to the coaxial setup and multirotor-specific issues such as blade separation gap. The subject of this study is to explore variations that can be made to a strictly coaxial system to provide thrust as much as possible like a similar system of independent propellers.

## 1.2 Theory

From the literature reviewed in the section above, it is sufficiently understood that flow interactions result in thrust losses for downstream rotors. The faster air entering the lower coaxial propeller cannot be accelerated as much as slow air would be, explaining the decreased thrust in the system. Slight increases in drag may also be experienced by the lower motor, reducing the registered thrust<sup>26</sup>. For individual rotors, relationships have been long-established between thrust, torque, power, efficiency, and rotor speed. In Figure 5, Merchant<sup>20</sup> provided a graphical representation of how efficiency ( $\eta$ ) and dimensionless coefficients of thrust ( $C_T$ ), torque ( $C_Q$ ), and power ( $C_P$ ) vary with advance ratio ( $J$ ).

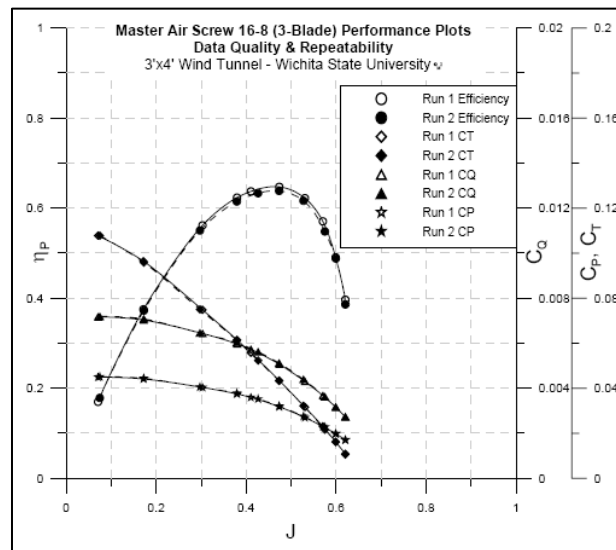


**Figure 5.** Performance plots show trends between variables and prove repeatability.<sup>20</sup>

Advance ratio perpendicular to the propeller disc is defined by Leishman<sup>32</sup> as a dimensionless representation of propeller tip speed ( $\Omega R$ ) relative to the free stream velocity ( $u$ ). Merchant's plots are characteristic of established relationships between each variable and advance ratio.

$$\text{advance ratio: } J = u/\Omega R \quad \{\text{Equation 1}\}^{32}$$

One can combine Equation 1 and Figure 5 to recognize that when the lower coaxial rotor experiences a significantly higher free stream velocity ( $u$ ) without proportionate increases in rotational speed ( $\Omega$ ), advance ratio ( $J$ ) increases considerably. According to performance plots, this has been observed to reduce the thrust, torque, and power coefficients for the system. These quantities can be translated with the variables of air density ( $\rho$ ), rotor disc area ( $A$ ), blade radius ( $R$ ), and blade tip speed ( $\Omega R$ ).

$$\text{thrust } T = \frac{1}{2} C_T \rho A (\Omega R)^2 \quad \{\text{Equation 2}\}^{32}$$

$$\text{torque } Q = \frac{1}{2} C_Q \rho A (\Omega R)^2 R \quad \{\text{Equation 3}\}^{32}$$

$$\text{mechanical power } P_{out} = \frac{1}{2} C_P \rho A (\Omega R)^3 \quad \{\text{Equation 4}\}^{32}$$

Air density ( $\rho$ ) can be assumed constant because the winds generated by the experiments were not strong enough to cause compression effects. The radius ( $R$ ) and disc area ( $A$ ) are also constant for rigid propellers. Tip speed ( $\Omega R$ ) is still considered to have remained constant. Hence, changes in coefficients can be considered as if they were changes in the thrust, torque, and power variables themselves. In summary, the faster incoming air for a downstream rotor results in the reduction of thrust from the rotor.

Equations 2-4 consider thrust, torque, and power from an aerodynamic perspective. For the scope of this study, an operational perspective is used. Rather than focusing on the relationships of dimensionless variables, this study concerns itself with relationships between thrust ( $T$ ), torque ( $Q$ ), electrical power ( $P_{in}$ ), and efficiency ( $\eta$ ).

Rotor torque is the connective tissue between thrust and power measurements. Prior<sup>29</sup> noted a linear relationship between thrust and torque values and used a constant factor ( $\kappa$ ) to substitute thrust for torque in the power equation.

$$\text{mechanical power: } P_{out} = Q\Omega = \frac{T}{\kappa}\Omega \quad \{\text{Equation 5}\}^{29}$$

In the above equations, the factor  $\kappa$  is used to represent the experimentally-determined slope of linear relationship between thrust and torque for a certain propeller. This value is defined for each propeller in the Calibration section below.

The electrical power ( $P_{in}$ ) is calculated as the product of the measured current ( $i$ ) and voltage ( $V$ ) supplied to the system.

$$\text{electrical power: } P_{in} = iV \quad \{\text{Equation 6}\}$$

Using mechanical and electrical power, the system's efficiency can be calculated. Efficiency is a useful dimensionless metric for comparing systems. A higher efficiency in this context indicates that a system is better at converting electrical power into rotor torque and rotation.

$$\text{efficiency: } \eta = P_{out}/P_{in} \quad \{\text{Equation 7}\}$$

Efficiency is not a perfect metric for this study. In a coaxial setup, drag from the upper coaxial rotor's wake can induce rotation in a downstream rotor. When a propeller spins without generating thrust, it

is not calculated to be outputting any power. Similarly, a propeller generating low amounts of thrust can spin quickly when in a high-speed wake and would be calculated to be outputting more power than it actually is. To represent thrust generated as a result of electrical power, a new term was introduced, a ratio of thrust generated by the rotor to the power consumed by the rotor. For brevity, this was termed as “performance” ( $\Pi$ ):

$$\text{performance: } \Pi = T/P_{in} \quad \{\text{Equation 8}\}$$

Performance values effectively communicate how well the rotor is converting electricity to thrust. This includes the two terms of highest concern to UAV designers. As explained, the rotational speed of the rotor can be confounding to efficiency calculations in coaxial setups.

The coaxial thrust reduction is directly linked with the faster air passing through each successive propeller. Blade element theory allows for each rotor cross-section to be evaluated individually. For any cross section at any radial position ( $r$ ), the propeller is an airfoil, as represented in Figure 6, positioned with an angle of incidence ( $\alpha_1$ ) relative to the solid horizontal reference line. The airfoil moves from right to left and the airflow over the section is represented as the element’s in-plane speed ( $r\Omega$ ). Because the air flow over the airfoil is horizontal, the airfoil’s angle of attack is  $\alpha_1$ . Likewise, the airfoil section produces aerodynamic thrust ( $L_1$ ) and torque ( $rD_1$ ) on the rotor:

$$\text{blade element thrust (} u = 0 \text{): } T_1 = L_1 \quad \{\text{Equation 9}\}$$

$$\text{blade element torque (} u = 0 \text{): } Q_1 = rD_1 \quad \{\text{Equation 10}\}$$

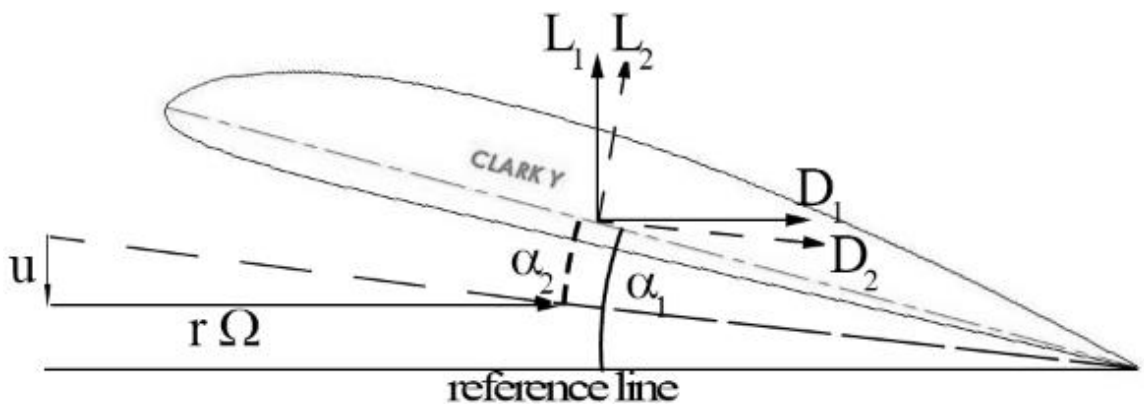


**Figure 6.** For any propeller’s airfoil, a higher advance ratio ( $u/r\Omega$ ) reduces the effective angle of attack ( $\alpha_{1,2}$ ) at every cross-section. This reduces the effective pitch of the propeller and makes it less effective.

With the introduction of a downward airspeed vector ( $u$ ), the aerodynamics change. The airfoil is now moving relative to the resultant air flow vector, indicated in Figure 6 by the dashed arrow. The airfoil's angle of attack is now with reference to the dashed line,  $\alpha_2$ . With a lower angle of attack, the lift ( $L_2$ ) and drag ( $D_2$ ) generated are not only less than before, they are at an angle. The thrust and torque are now represented by the equation:

$$\textit{blade element thrust } (u > 0): T_2 = L_2 \cos \alpha_2 - D_2 \sin \alpha_2 \quad \{\text{Equation 11}\}$$

$$\textit{blade element torque } (u > 0): Q_2 = r(L_2 \sin \alpha_2 + D_2 \cos \alpha_2) \quad \{\text{Equation 12}\}$$

The thrust is now hampered and the torque is greater than before, which are problematic. To alleviate and adapt to this, each successive propeller could spin faster, increasing  $\Omega$  to lower  $J$  and bring the dashed line closer to horizontal, or have a higher pitch, increasing  $\alpha_1$  and thereby  $\alpha_2$ . Both of these approaches will be the basis of experiments within this study.

## 2. Experimental Setup

### 2.1 Equipment Details

To test the viability of a four-propeller coaxial setup, experiments were conducted wherein the motors were attached to the ends of aluminum rods which extended one foot off the edge of a table. This is visible in Figure 7. Components are labeled for reference within this section. Rotors (“A”) are mounted on load cells suspended at the end of the support rods. A power supply (“B”) provides steady DC power to the system. A multimeter (“C”) is used to calibrate current sensors in the data acquisition system (“F”). Electronic speed controllers (ESCs) (“D”) are connected to the rotors, the power supply, and the servo tester (“E”). A handheld laser tachometer (“F”) is used to reassure rotor speed using the reflective tape on each motor.

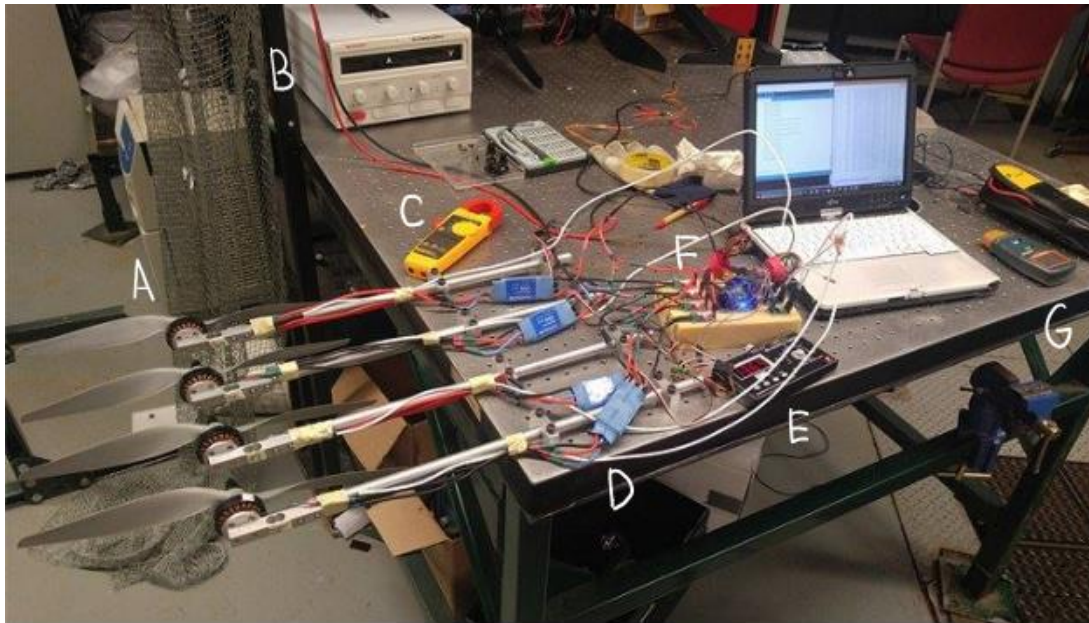


**Figure 7.** Experimental setup for four coaxial rotors, support hardware, and data acquisition equipment.

In all experiments, the motors, ESCs, and power supply were unchanged. By using the same equipment to run each propeller, the effects of the propellers could be better isolated. To provide insight for a project under development in the lab, an unmanned multi-medium vehicle called “The Naviator”, tests began with the same propeller, motor, and ESC used onboard this vehicle.

T-Motor MN4006-23 380KV brushless DC motors used to drive the propellers. Before experiments were conducted, eight motors were evaluated for consistent behavior. The manufacturer claims that with the T-Motor 13-inch diameter, 4.4-inch pitch carbon fiber propeller, the motors could produce 1633 grams-force of thrust, reach 6515 revolutions per minute (RPM), and produce 0.267 newton-meters of torque. On average,

the consistency tests provided 1080 grams-force of thrust, reached 6135 RPM, and provided 0.176 newton-meters of torque. Standard deviation in thrust across eight motors was only 2%. The four motors that were chosen for future tests were the ones that showed most consistent performance by falling within one standard deviation of the average across the aforementioned measurements.

It can be noted here that although the gram-force is not a standard unit as dictated by the *Système International (SI)*, it is commonplace to use these units in propulsion contexts. Multiple reputable organizations and journals allow for the use of gravitational force units<sup>18,19,20,24,28,29,30</sup>. With respect to this convention, thrust measurements are provided in grams.

The ESCs were preloaded with identical firmware. They operate at voltages up to 33.6V and continuous currents up to 45A. The power drawn during the experiments would never exceed this limit. To reduce undue interference in the propellers' wakes, the ESCs were stationed at the table's edge and extension wires leading to the motors were taped to the back of the rods, as visible in Figure 6.

Although in practice a vehicle implementing electric motor-driven propulsion would be powered by a battery, a Maisheng DC Power Supply was used in tests because it can provide a constant voltage and current. To simulate a six-cell lithium-polymer (LiPo) battery, voltage could have been set in the range of 19.8V to 25.2V. For all tests, operating voltage was 24.0V DC to provide the operating characteristics of a battery at approximately three quarters of a full charge.

The propellers were a varied component in the system. For the main experiments, carbon fiber propellers from T-Motors were used. Their diameter was 13 inches and their pitch was 4.4 inches. An illustration helps to understand the physical implications of these values. Figure 7 features an airplane flying from right to left. The black sinusoidal curves represent the path of a blade's tip for one revolution. A good analogue for a propeller is a wood screw. When rotated once, its thread advances the screw by a specific distance, its pitch. For a rotor, this is the geometric pitch. Due to the low viscosity of air, slip occurs and a rotor only advances by an effective pitch. The diameter of the propeller is measured from tip to tip and can be visualized as the height of the black curves in Figure 8.

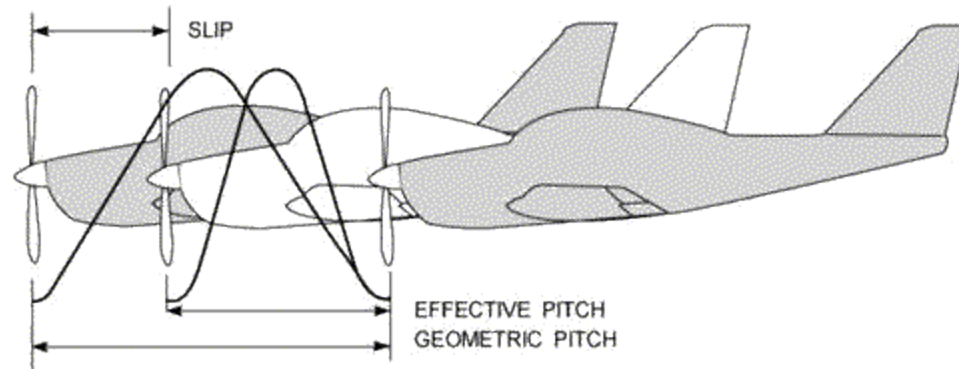


**Figure 8.** Pitch of a propeller, illustrated in the context of a fixed-wing aircraft.

For experiments in which the effects of pitch were explored, glass fiber composite propellers from APC Propellers were used. These had a 13-inch diameter, ranged in pitch from 4 inches to 10 inches and had consistent design, in which an Eppler E63 airfoil blends with a Clark-Y airfoil. Any imbalances in the propellers were addressed before use by removing material on the lower surface of the blades.

To measure thrust and current, a data acquisition system (DAQ) was assembled using an Arduino Uno R3. Thrust was measured by mounting the motor onto a load cell with strain gauges connected to a HX711 load cell amplifier, which discretized the analog resistance change into digital values. The Arduino then read the load cell amplifier and scaled its measurement to gram-force units. The load cells used were rated for up to five kilograms. Scaling factors were determined by calibrating each load cell and amplifier pair with four different loadings.

Current was measured using Fluke 325 Clamp Meters, which use inductance to measure current flowing in a wire. These were replaced with ACS712 current sensors, which fed raw data to the Arduino to be properly scaled to match the Flukes' readings.

To specify the duty cycle setting for any test, a servo tester was used to produce a pulse-width modulated (PWM) signal. At the beginning of each test, the ESCs were calibrated to the extreme values of the generated signal. This teaches the ESC the minimum and maximum cycle periods of the PWM signal so that it can interpolate corresponding throttle settings to the proper duty cycle.

Motor speed was measured using a handheld DT-2234C+ digital laser tachometer and reflective tape. The device was directed to shoot a beam of light at the motor's bell. The reflective tape signaled a revolution and the rotor speed was displayed on a digital readout. The tachometer was held approximately

eight inches from the motor. Although values would vary before stabilizing, minor variations of  $\pm 10$  RPM are minor considering typical values 4000-7000 RPM.

A review of measurement equipment accuracies and resolutions is included in Uncertainty Analysis.

## 2.2 Calibration

For the most precise data, thrust-measuring and current-measuring equipment were calibrated at the beginning of each test. Steel blocks of known weight were placed upon the load cell to confirm proper scaling. When processing the data later, recorded measurements at zero load were subtracted from thrust measurements to eliminate bias. Also during data processing, outliers in the data as a result from randomly erroneous readings were deleted. Examples include values in excess of one thousand when all other measurements center around sixty. Such instances were rare, but were familiar to the author from previous Arduino projects without strong low-pass filters.

The current sensors were calibrated by running a motor and propeller at different throttle settings. The average of recorded values was plotted against indicated value on the Fluke, down to the hundredths place. A linear trendline fit the data well and its slope was used to correct data. Similar to thrust data, initial measurements were deducted when all of the data was being processed.

Separate from the experiment, propellers were tested on a torque sensor and load cell. The data from these tests provided a linear relationship between torque and thrust in which the trendline's slope enables conversion between grams-force and millinewton-meters. The conversion factors' values are tabulated below:

Diameter (inches)	13	13	13	13	13	13
Pitch (inches)	4	4.4	5.5	6.5	8	10
Material	Glass fiber composite	Carbon fiber composite	Glass fiber composite	Glass fiber composite	Glass fiber composite	Glass fiber composite
Factor $\kappa$ (g/mN-m)	7.758	6.180	6.570	5.959	5.605	4.608

**Table 1.** Six different propellers are used in experiments and each has a different factor.

The values from Table 1 are used in Equation 5 to calculate the mechanical power of each propeller. For the glass fiber composite propellers, this factor (which is a divisor<sup>29</sup>) decreases with increasing pitch values, indicating that spinning higher-pitch rotors requires more torque.

### 2.3 Experimental Procedure

Before each test, support rods and propellers were tightly secured to reduce vibrations. ESC connections were checked to avoid shorting the system or spinning any rotors backward. At the throttle settings predetermined for each experiment, thrust, current, and motor speed data were collected. Then, the servo tester would be dialed to the next desired throttle setting or reach the desired current draw.

### 2.4 System Diagrams

A goal of this research was to explore the effects of coaxial propeller setups. Such a setup involves a series of motors and propellers positioned directly behind one another. The disturbed air from the leading propeller influences the performance of each propeller thereafter. In the scope of this experiment, up to four propellers were tested in a coaxial setup, as shown in Figures 7 and 9. In figure 9, a diagram of the rotor configuration is introduced.

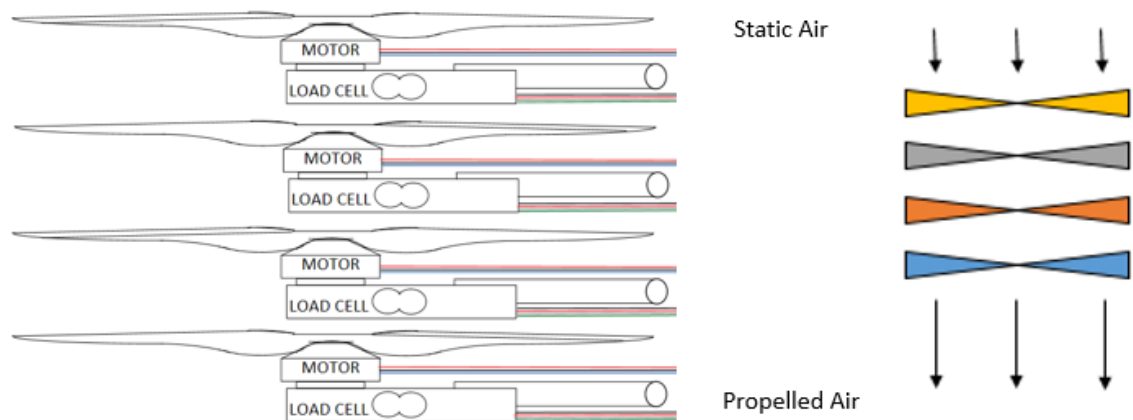


**Figure 9.** The arrangement of propellers, one behind another, is established for the reader. A simplified diagram of the propellers and air flow is provided for its relevance in relation to later plots.

The rotors in Figure 9 pass the air from the upper propeller downward. This is represented by the arrows characterizing the direction of air flow from the first (yellow) rotor to the second (gray), third (orange), and fourth (blue) rotors. During tests, rotors were not on parallel horizontal planes as Figure 9 may suggest, but on parallel vertical planes as Figure 7 shows.

The components listed in the section above are included in the diagrams below. In this setup, each identical propeller is provided the same voltage and throttle setting. Figure 10 is a complete diagram of the wired connections between the components in Figure 7.

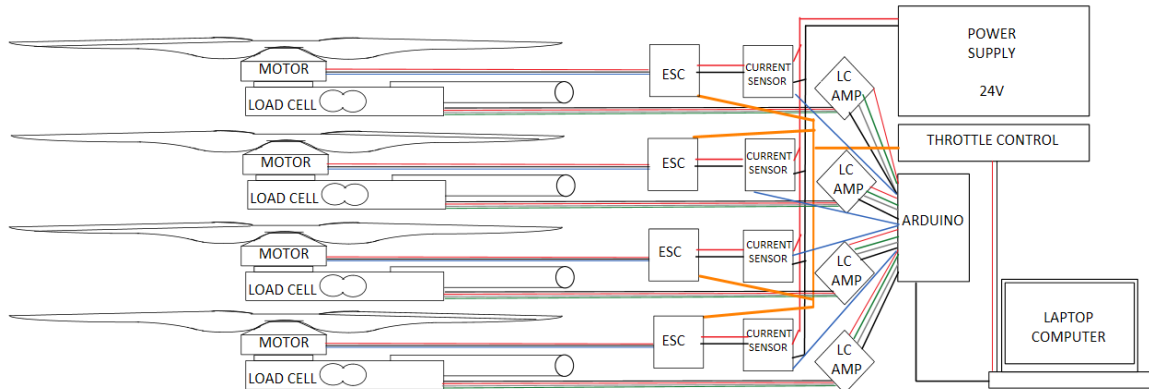


**Figure 10.** The four coaxial propellers, each with connections to power, control, and measurement systems. This setup shows the thrust and current changes associated with a system of more propellers at various distances.

This diagram does not specify distance between consecutive propeller planes of rotation because it is a variable considered in a set of experiments that sought to isolate the effect of separation distance. Another set of experiments operates fewer than the illustrated number of propellers, taking into consideration the system when only one, two, or three motors are running. This test served to consider how an individual propeller's behavior might change based on how many propellers are present in the system.

To isolate the effect of propeller pitch in any pair of coaxial propellers, the experiment illustrated in Figure 11 was conducted. In this experiment, one hundred permutations of propellers were evaluated. In this setup, the motors are provided the same voltage and throttle setting. The distance between the motors in pitch experiments was 4 inches.

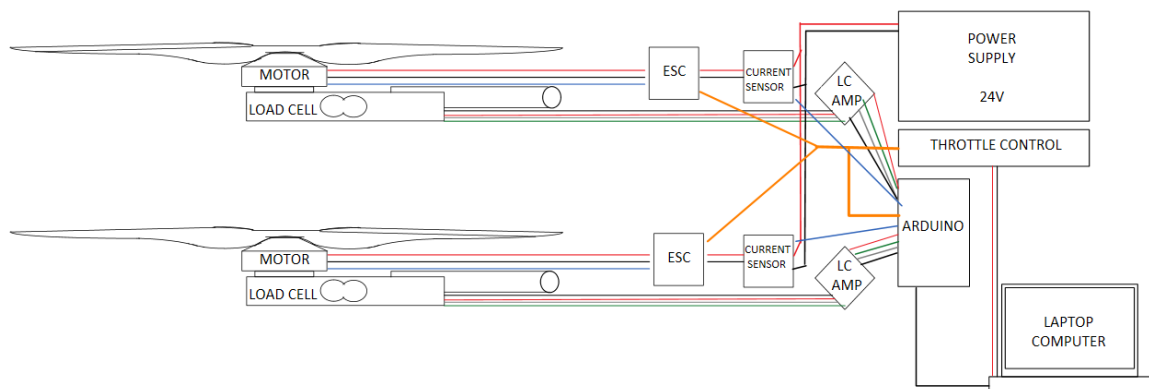


**Figure 11.** Propeller arrangement for isolating the role of pitch in a coaxial pair with testing equipment.

In order to evaluate the effect of differing throttle settings in any pair of coaxial propellers, an experiment was conducted which provided independent throttle control on each of the motor. In this

experiment, identical propellers are tested. The setup in Figure 12 resembles the diagram in Figure 11, but includes the second throttle control unit.

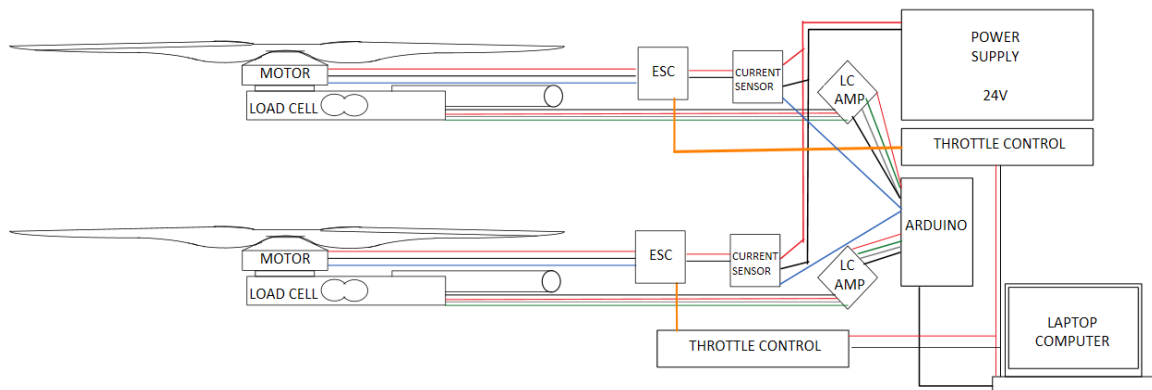


**Figure 12.** Propeller arrangement for isolating the role of throttle and motor speed in a coaxial pair with testing equipment.

## 2.5 Uncertainty in Measurement Equipment

Thrust measurement begins with the load cell, produced by Uxcell. The load cell has a zero balance uncertainty of  $\pm 2\%$  F.S., which is an uncertainty of 100 grams for the zero load point. The load cell is sensitive to temperature and has an uncertainty of less than  $0.005\%$  F.S./ $10^\circ\text{C}$  with a rating up to five kilograms, causing an uncertainty of 250 milligrams. An infrared thermometer reading before and after a test indicated the load cell temperature went from  $23.4^\circ\text{C}$  to  $26.7^\circ\text{C}$  through the duration of the experiment. This would account for 82.5 milligrams, a negligible quantity when measurements are one the kilogram scale. Due to the collection and deduction of values at zero load, a new baseline is established for each test. If the zero load point were to change during the test, that 100 grams would represent 9.09% of a typical thrust measurement.

The load cell's strain gauges vary resistance according to the magnitude of strain upon them, thereby varying voltage. These small variations are registered by a HX711 load cell amplifier. On this chip for a gain setting of 128, the typical offset drift is  $0.4\text{mV}$ , noise is  $50\text{ nV}$ , and temperature drift is  $\pm 6\text{nV}/^\circ\text{C}$ . The full scale range of the chip is  $\pm 0.5\text{V}$ , or  $1\text{V}$  scaling to raw values on a 24-bit range. Using a calibration scalar of 0.00285 grams per raw value increment, single millivolt equates to 47.815 grams of thrust. If these errors stacked during an experiment and the temperature changed with the load cell, then the value of maximum thrust could potentially be  $\pm 22.5$  grams biased. When maximum thrust values recorded are typically 1100 grams, error from the load cell amplifier constitute 2.04% error on the measurement.

The ACS712-30A current sensor module is a self-contained module with  $\pm 1.5\%$  total output error. The highest output value measured was 9.95A, yielding an error of  $\pm 0.149\text{A}$  at most for a single motor during these experiments. Across four sensors, that can amount to 0.596A out of 40A. Noise is typically 7 mV, which accounts for 0.11A at the minimum sensitivity of 63 mV/A. Noise represents 1.12% of the current.

As previously mentioned, bias was limited by taking baseline data each time the motors were powered on. Additionally, random error and noise were reduced by averaging at least fifty data points for thrust measurements. This practice is acceptable because during a motor's operation, the rotor is driven by the commutation of electromagnets on the stator. This occurs in pulses and perfectly smooth operation is impossible. Occasionally, outliers were measured in thrust without clear explanation. They were possibly the result of noise and interference within the unshielded connections of the data acquisition system. Outlier data were removed such that the standard deviation of every thrust measurement did not exceed thirty grams.

Human error could have entered the experiment during the collection of motor speed data using the handheld tachometer because each used data point was a single point, accurate to  $\pm 0.05\%$ . Although averaging was not done with collected data, it is certain that a moving average filter is incorporated into the tachometer's programming to provide stable measurement readouts and adjust to new measurements. The same goes for data collected using the Fluke clamp meter for current data collection, which is accurate to 2% of the measured value.

## 2.6 Considering Vibrations

Each motor is supported by a support rod, constituting a cantilever beam with a mass on the end. Such an equipment setup is vulnerable to vibration. Although vibrations did briefly occur during tests between 50% and 75% throttle, they subsided quickly and were not problematic. Each rotor support rod is made of aluminum 6061 with a modulus of elasticity around 69 GPa, radius of a quarter-inch (6.35mm), and a foot-long overhang (304.8 mm). The mass on the end comprises the 68-gram motor and the hardware necessary to attach to the rod and the propeller, estimated 100 grams in all.

$$f_n = \frac{1}{2\pi} \sqrt{\frac{3EI}{mL^3}} = \frac{1}{2\pi} \sqrt{\frac{3(69 \text{ GPa})\left(\frac{\pi}{4}(6.35\text{mm})^2\right)}{(100\text{g})(304.8\text{mm})^3}} = 7658 \text{ Hz} \quad \{\text{Equation 13}\}$$

Motor speeds never passed the low seven thousand revolutions per minute so a disturbance would have to occur about sixty times every revolution to incite vibrations due to the cantilever beam.

### 3. Results

#### 3.1 Four Coaxial Propellers

When studying the coaxial setup, it is with the goal of reducing the inevitable losses incurred in the downstream propellers. The first step in this process is to properly understand this effect, a test must be repeated between one and four rotors, as summarized in Table 3. This was performed with propellers that alternated spin directions and propellers that held consistent spin directions. This would allow for the understanding of how swirl in the airflow impacts the operation of downstream propellers. Tests were performed with motors eight inches apart.

	4 Alternating	3 Alternating	2 Alternating	1 Alternating	4 Consistent	3 Consistent	2 Consistent	1 Consistent
First Motor	CCW	CCW	CCW	CCW	CCW	CCW	CCW	CCW
Second Motor	CW	CW	CW		CCW	CCW	CCW	
Third Motor	CCW	CCW			CCW	CCW		
Fourth Motor	CW				CCW			

**Table 2.** A test matrix summarizes the spin directions of the rotors during the tests, clockwise (CW) and counter-clockwise (CCW).

The measurements from the alternating tests were totaled for each trial. To understand the effect of adding the fourth rotor (blue), the total thrust of three alternating rotors was subtracted from the total thrust of four alternating rotors, and so on. This series of tests was repeated three times, as shown in Figure 13.

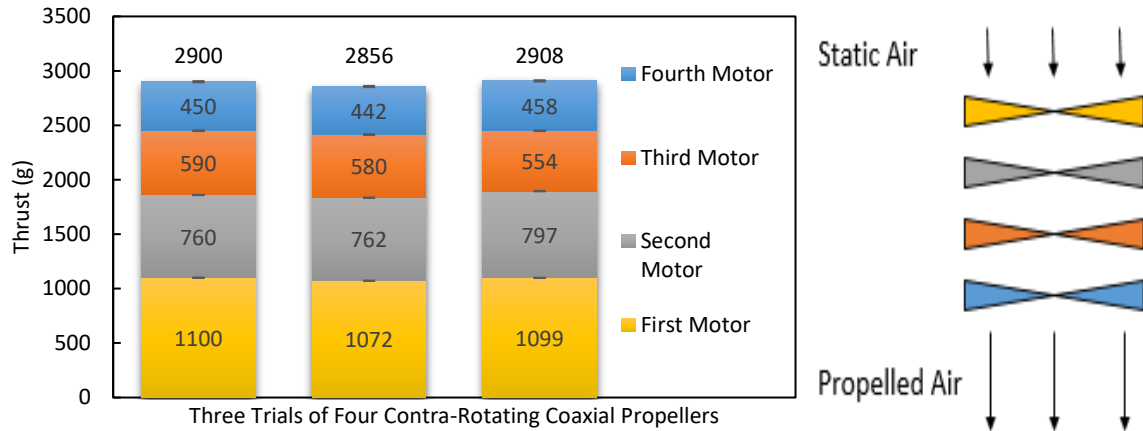


**Figure 13.** Thrust contribution of each 13”x4.4” contra-rotating propeller were isolated. This establishes a pattern of how thrust degradation continues downstream.

When three trials were performed with alternating propeller spin directions, the first propeller produced an average of 1090 grams of thrust. On average, each subsequent propeller produces 71%, 53%, and 41% of that thrust. This is visually represented as a stacked bar graph with the system’s total thrust indicated above each stacked bar graph.

Error bars for individual rotor thrust measurements were calculated using a t-distribution at 95% confidence for each measurement and may be difficult to see in Figure 13 because they reached as high as 5.7 grams and are presented on a scale of thousands of grams. Maximum errors on the total measurements were 12.2, 12.9, and 11.6 grams, respectively. The error bars of the outer two trials’ graphs overlap. For the average thrusts, the error bars were 39, 76, 50, and 69 grams for the first through fourth rotors.

To note the benefit of swirl recovery as the system progresses to four rotors, the total thrust of the four-rotor systems can be compared. In Figure 14, thrust measurements are summarized for three trials of co-rotating coaxial rotors. Although thrust degradation for downstream continues, they are not the same as in Figure 13.

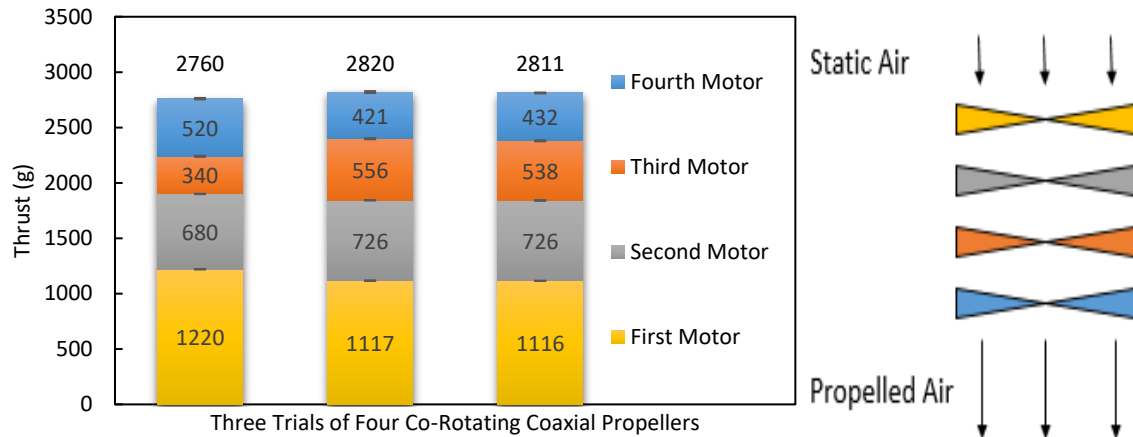


**Figure 14.** Thrust contribution of each 13''x4.4'' co-rotating propeller isolated. The total thrusts are summarily lower than the total thrusts of Figure 13.

When three trials were performed with consistent propeller spin directions, the first propeller produced an average of 1150 grams of thrust. On average, each subsequent propeller produces 61%, 42%, and 40% of that thrust. This is visually represented as a stacked bar graph with thrust totals above each trial's bar graph.

Error bars were up to 8.8 grams for individual rotor thrusts, which may be difficult to identify on the given scale. The error bars on the two rightmost graphs overlap. Maximum error bars on total thrust were 14.9, 16.8, and 13.1 grams, respectively. Error bars overlap occurs for the two rightmost bar graphs. For the average thrusts, the error bars were 150, 83, 215, and 80 grams for the first through fourth rotors.

The 60-gram difference in the first propeller's average thrust seems incidentally related to the measurements in the first trial. It represents a 5.5% difference relative to the 1090-gram measurement. On the whole, however, total thrust values seem to all inhabit the same neighborhood for both alternating- and consistent-direction setups, indicating the minor role of swirl in the system's operation. This minor impact does support the implementation of alternating propellers in a coaxial arrangement. The contra-rotating setup appears to be most advantageous for the first pair, though its benefits continue to the following propellers.

With its losses identified, it is important to compare the coaxial system to its opposite, a multi-axis system in which each successive propeller is alongside the other propellers. In such a system, all the propellers are receiving clean airflow and operate as an individual propeller. The difference is illustrated below.

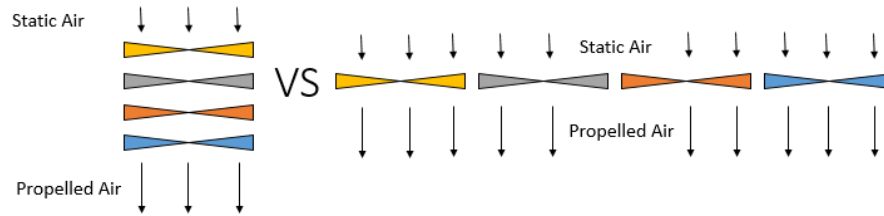


**Figure 15.** Simplified diagrams representing coaxial (left) propeller configuration and multi-axis (right) propeller configuration. Multi-axis propellers operate independently and produce equal amounts of thrust.

The thrust from a multi-axis setup is modeled linearly, as shown in Figure 16, with respect to the number of motors in operation and current draw. Since the multi-axis setup does not suffer the same losses inherent in a coaxial setup, it will always provide more thrust but it will also increase the footprint of the vehicle. The coaxial plot represents the average thrust values and total error bars based on the average errors of each rotor in each trial. The total error bars are 1.3, 3.1, 6.5, and 12.3 grams for coaxial systems with one, two, three, and four rotors, respectively. Error bars for the multi-axis setup were created by multiplying the error from a single rotor by the number of rotors, reaching 5.3 grams.

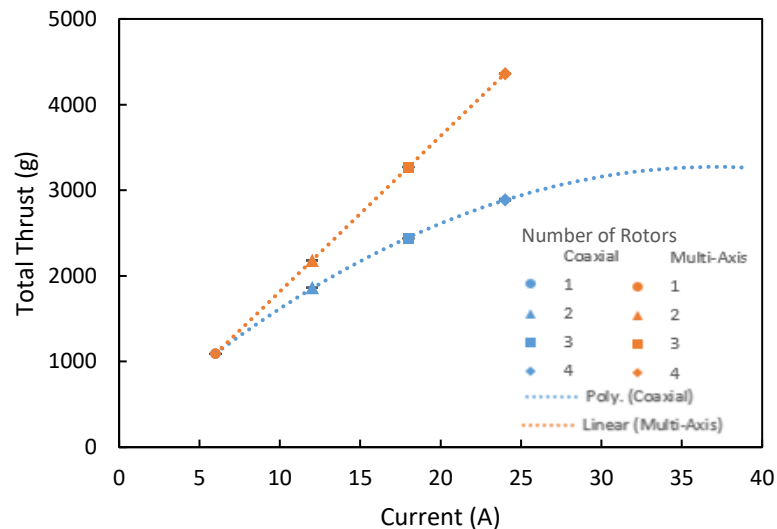


**Figure 16.** Total thrust of coaxial and multi-axis systems compared. Because the coaxial system produces decreasingly more thrust with each additional propeller and the multi-axis system produces equal thrust with added propellers, the gap between the thrust generation curves continues to grow.

As the number of operating propellers increases, so does the deviation between coaxial and multi-axis models. The coaxial model follows a polynomial trend which is expected to peak at 37.15A according

to the trendline's equation. Based on the fact that the system is provided 6A for each motor, this peak is approximately the current of six motors running at their maximum throttle setting. A seventh motor would not be expected to contribute thrust due to the high speed of incoming air and multi-rotor designers would not add that additional rotor. If a coaxial set were to operate at the point that total thrust reaches its peak, the total thrust would be 3273 grams, or 312% the thrust of a single 13"x4.4" propeller on this motor.

In Figure 17, the coaxial-to-multi-axis thrust ratio is represented for each successive rotor. This is only based off of the model of multi-rotor vehicles acting like isolated rotors. Literature clarified that that is not entirely true due to interactions between rotors<sup>22,23,27</sup>. The linear model is still useful for comparisons, idealized as it may be<sup>27</sup>.

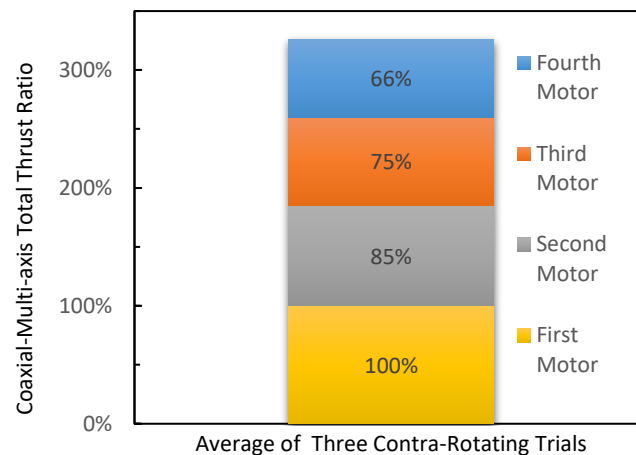


**Figure 17.** Total thrust values for coaxial system divided by corresponding total thrust values of multi-axis system according to how many motors in the system. Represents considerable disadvantage to coaxial setup.

A coaxial setup is capable of providing a fraction of the multi-axis system's thrust. With two motors, a coaxial motor setup will be 85% as effective as a pair of motors on separate axes of rotation. A designer of multirotor vehicles would be able to use ratios such as this if they were constrained into a coaxial design.

To test the consistency of the ratios comparing downstream rotors to the first rotor, the experiment was repeated with the APC Propellers 13"x10" thin electric propeller. Propellers of high pitch are typically not used for multirotor vehicles, but for fast-flying airplanes. Having a higher pitch on downstream propellers did more than provide more thrust at the expense of more power. Figure 18 includes a thrust-ratio graph like Figure 13 and a multi-axis comparison graph like Figure 17. For total thrust measurements, errors were 1.3, 4.4, 5.2, and 7.6 grams for one, two, three, and four rotor systems.

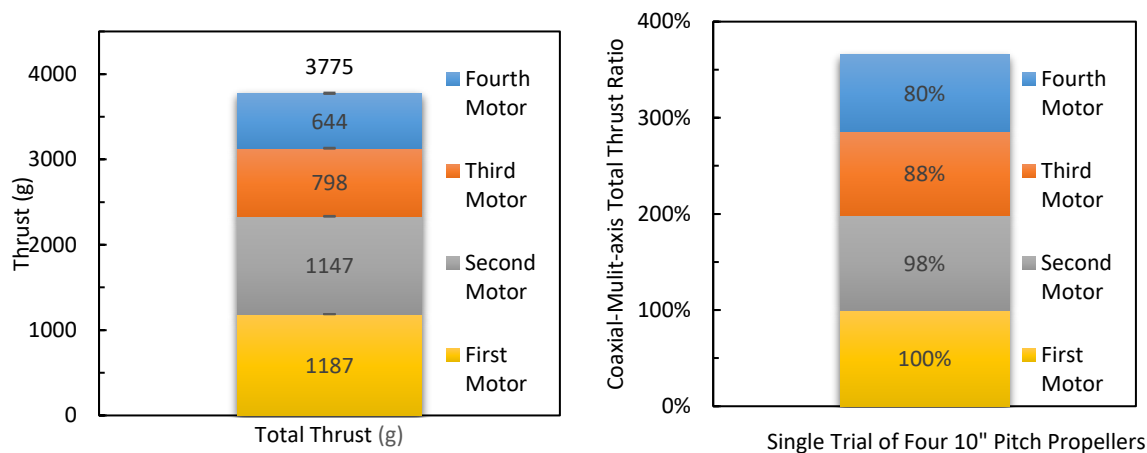


**Figure 18.** Using four 10-inch pitch propellers provided more thrust overall, especially since the second propeller produces as much thrust as the first propeller. This improved the comparison with a multi-axis system.

The higher pitch delays the deviation from the multi-axis model as the two-rotor coaxial system provides 98% of the thrust of the two-rotor multi-axis system. In the case of this propeller, the downstream propellers' thrust contributions are 97%, 67%, and 54% that of the first propeller. This shows that the thrust ratios from before are not true for every propeller. Of course, it is important to match propellers and motors and to take into account airspeed. When the air passed the first propeller, it was still at a speed acceptable to the second propeller and significant losses were not observed until the third propeller. Even if the first motor was underperforming as evidenced by slower air, it seems that the second motor was operating well. The third motor provides 70% of the second motor's thrust and the fourth motor provides 56% of the second motor's thrust. These are much closer to the previously observed thrust contribution ratios.

The performance of a propulsion system can be quantified as the thrust received per unit of consumed power, in units of grams per watt, as described in Equation 8. For the multi-axis model, it is assumed that both thrust and power consumption will be equal across motors, providing a horizontal performance curve.

Average error bars from contra-rotating rotors were divided by the power usage of the system. For one, two, three, and four rotors, error bars were 9.2, 10.7, 15.2, and 21.3 mg/W. Error bars for all multicopter setups were 9.2 mg/W. Again, these values are small relative to the scale in grams per watt.

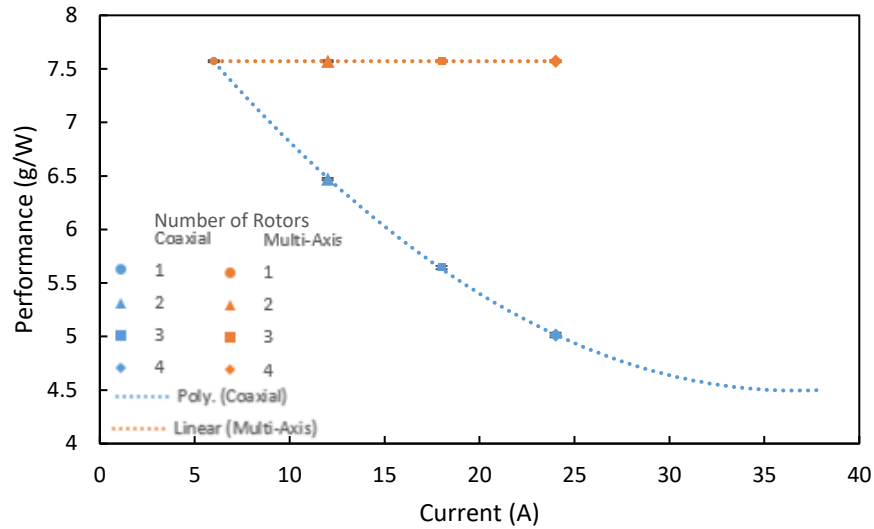


**Figure 19.** Performance (g/W) of the system descends sharply for a coaxial system with four 13''x4.4'' propellers. As more propellers are added, successive performance reductions are less.

Performance of the coaxial system descends along a path that adheres to a polynomial fit. Projecting the data forward suggests that the performance will reach its minimum at 36.3A. This suggests that the performance metric should plateau at 4.53 grams per watt for the subjunctive six coaxial rotors considered earlier.

The declining performance of a coaxial system is symptomatic of decreasing system efficiency as additional propellers are introduced. The power into the system is simply the product of total current draw and supplied voltage, which was held at 24V. The power output is the product of motor torque and motor speed. The torque is derived from thrust values and the appropriate conversion factor  $\kappa$  in the Calibration section. As evidenced by the decreasing slope of the coaxial power curve, the efficiency of the coaxial system decreases as more motors are added.

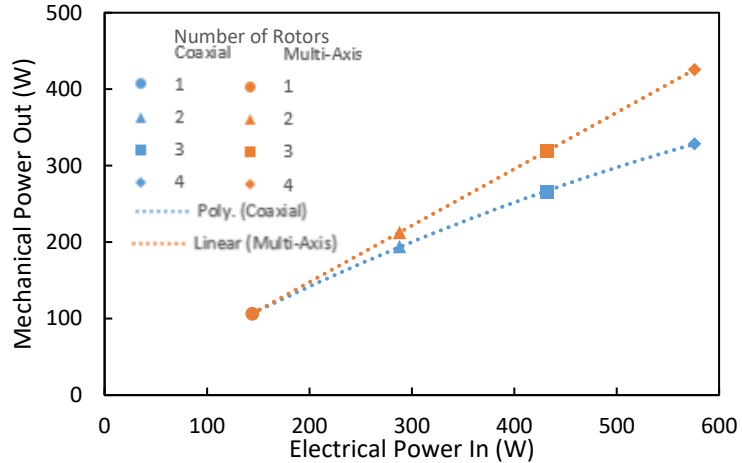


**Figure 20.** Coaxial and multi-axis systems’ power curves can be analyzed for efficiency. The slope of the coaxial curve reduces as additional propellers are added to the system, indicating reduction in efficiency.

With a baseline of four coaxial rotor systems, variations on the setup are introduced. The distance between propellers’ planes of rotation varied from two-inch separations to eight-inch separations. At eight inches, the system stretched over 32 inches meeting spatial constraints on the test area. Because contra-rotating rotor configurations were more consistent and provided more thrust, propellers alternated spin directions. Tests were repeated at two-inch intervals. In Figure 21, thrust stacks akin to Figure 13 were produced for these distances.



**Figure 21.** Separation distance was altered and the experiment associated with Figure 7 was repeated. Between two and eight inches of separation between propellers’ planes of rotation, little change is observed.

Within the range tested, there was no significant difference between systems' thrust values. The ratios of individual thrust contributions are consistent with previous data. Previous tests separated propellers by 8 inches and in closer setups, the thrust produced by each rotor is consistent across different separation distances. The error bars in Figures 21 and 22 were calculated for each rotor at each distance. Individual errors did not exceed 6 grams of thrust. Total thrusts had maximum errors of 9.45, 7.54, 8.64, and 14.73 grams for two, four, six, and eight inches of separation, respectively. Total thrust error bars overlap between two- and four-inch separation distance graphs.

Figure 22 plots the total thrust of the system as each rotor is added. By comparing the data on the same graph, the plots can be seen to overlap for the most part.

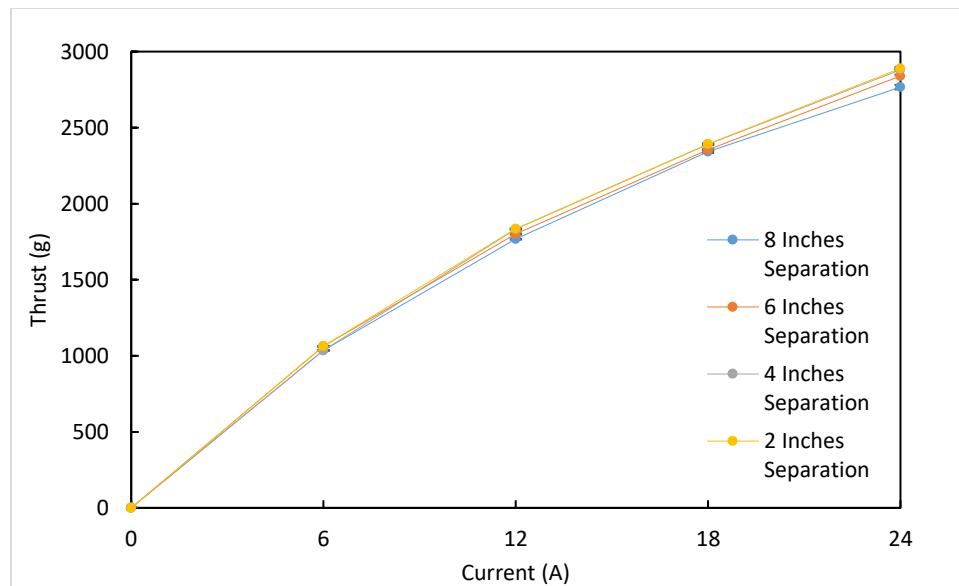


**Figure 22.** Minor improvements are noticed with closer propellers when total system thrust is plotted against total current. The advantage of closer propellers becomes more apparent with more motors.

The separation of plots manifests as more propellers are added in favor of smaller separation distances. At 6A, the system with 2-inch spacing is 2.5% more efficient than the system with 8-inch spacing. At 12A, it is 3.9% better and at 24A, it is 4.5% better. These differences in total thrust affirm previous research that indicated improved operation at closer inter-planar distances<sup>26</sup>.

Thrust values were divided by the electrical power of the system to yield performance values. In Figure 23, the system performance is plotted for different numbers of motors. Values for performance of a single motor have about 0.2 g/W deviation. This spread is the result of randomness in the experiment. When

more motors are added, performance values are still spread but an order exists wherein curves representing closer rotors perform better than those of distant rotors. This suggests that the spread can be attributed to the closer systems performing better.

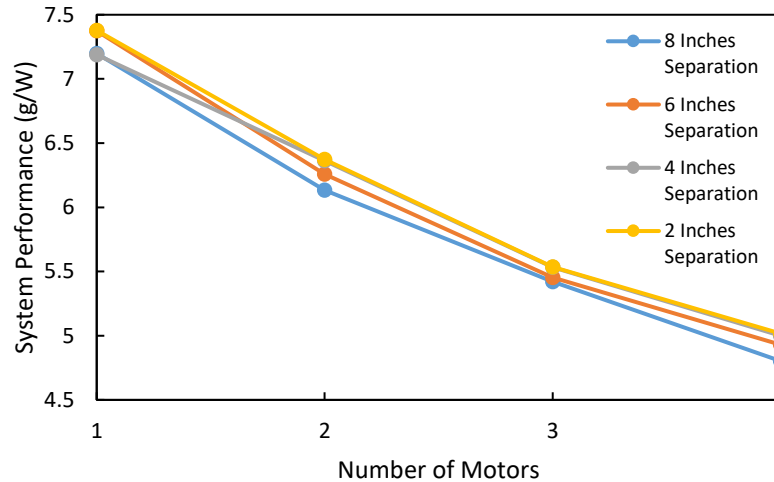


**Figure 23.** Performance of the system is best when the propellers are closer.

The collected data also indicate in the figure above that the system's performance drops with each additional motor and each increase in separation distance. Error bars in the system performance values were 16.4, 13.1, 15.0, and 25.6 mg/W in order of increasing distances. Error bars are so small relative to the other values that they are eclipsed by data markers in Figure 23.

In efforts to reduce the thrust loss inherent to a set of four coaxial propellers, this section has considered the effects of rotor spin direction and distance between rotors' planes of rotation. From these exercises, contra-rotating systems were deemed slightly preferable to co-rotating systems. Also, the coaxial system performed slightly better when rotors were positioned in close succession.

### 3.2 Two Coaxial Propellers of Different Speeds

Because thrust is related to propeller tip speed squared according to Equation 2, a slightly faster downstream propeller is the first method to explore for reducing the thrust losses of a coaxial rotor. As explained in the Figure 12, individual control of the two motors was achieved by implementing two identical servo testers to provide two separate PWM signals to the ESCs. To reduce the volume of data collected, the back motor was only advanced in 25% throttle increments while the front motor was advanced in 12.5% increments.

In a coaxial setup, the thrust of a downstream propeller is not the only thing affected by its predecessor, the rotational speed of the propeller and motor is also affected. This is visible when windmilling, the passive rotation of an unloaded rotor, occurs. In Figure 24, windmilling can be observed for the final three points of the 0% Throttle curve. In this figure, each line represents the back motor speed when the back motor's PWM signal is held constant and the front motor's signal is brought from bottom to top.

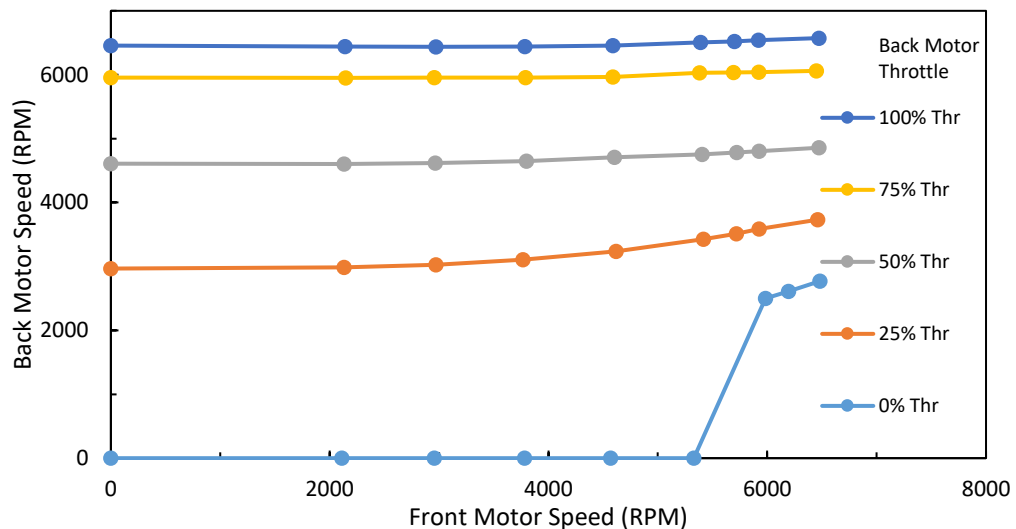


**Figure 24.** Back motor speed is clearly affected by the front motor speed variable. However, the vertical alignment of nearly all data points indicates no reciprocal effect on front motor speed.

Figure 24 shows that the interplay of the motor speeds is one-sided. The data points on each curve are mostly aligned vertically with the corresponding points on other curves. This shows that as back motor throttle changes, the same front motor throttle setting will spin the motor at a consistent speed. However, the back motor's speed is prone to the influence of the front motor. Back motor speed climbs gradually along each curve as front motor speed increases. That is, the front propeller helps to spin the back motor slightly. This increase becomes more subtle as back motor throttle increases and its onset appears to be more delayed.

Because the experiment measures the thrust from each propeller, the effects of motor speeds on each rotor's thrust can be studied, as in Figures 25 and 26. For the most part, the front propeller's thrust output is not affected by the back motor. The exception occurs as minor differences between curves at lower speeds. As front motor speed increases, the minor influence of back motor throttle becomes invisible and the curves converge to 1220 grams at 6500 RPM. Error bars were calculated to be at most 0.6 grams for any thrust measurement of the front or back rotor at any throttle setting.

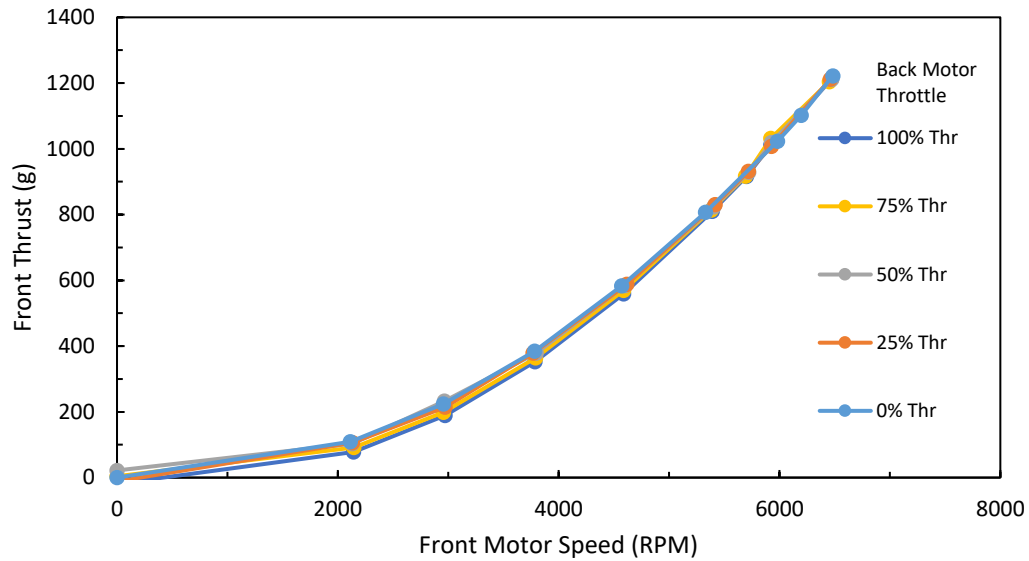


**Figure 25.** The thrust of the front motor directly corresponded to its speed and was unaffected by the back motor's speed.

Indeed, when the back motor is at lower throttle settings, the thrust of the front rotor is higher. As the back motor throttle increases, front thrust values drop slightly. The front rotor producing less thrust in a coaxial setup than a solitary rotor is documented<sup>8</sup>, but Figure 25 shows that this effect is only relevant up to a 50% front motor duty cycle.

In Figure 26, the thrust of the back rotor is plotted against the front motor speed. The plots all descend as a result of the increased front rotor thrust outlined in Figure 25. However, front motor speed is used as abscissa because it is directly controlled by the ESC.

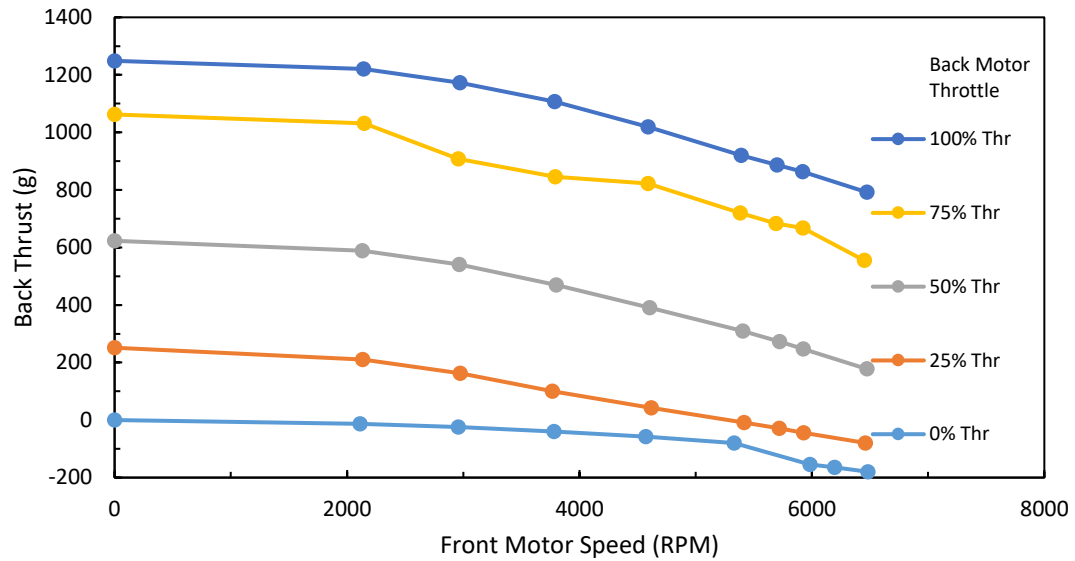


**Figure 26.** The thrust of the back motor clearly increased with its throttle setting but decreased according to the speed of the front motor. The thrust the back motor can be completely negated in some situations.

The thrust of the back propeller declines immediately due to the drag in the wake of the front propeller. The losses intensify at higher front motor speeds and can amount to about 500 grams. In the case of the 100% throttle curve, 35% of its thrust was lost to coaxial effects. In the case of the 25% throttle curve, all the thrust initially generated was negated by the drag of the front propeller, representing a coaxial loss greater than 100%. The back motor at 0% duty cycle, which does not begin spinning until approximately the front motor reaches 6000 RPM, immediately loses thrust faster when the wake begins to drive it to spinning.

Figure 27 plots the coaxial pair's total thrust and shows that the thrust a faster front motor generates eclipses the losses it imposes on the back motor. Indeed, the plots resemble the front rotor thrust curves positioned vertically according to the initial thrust of the back rotor.

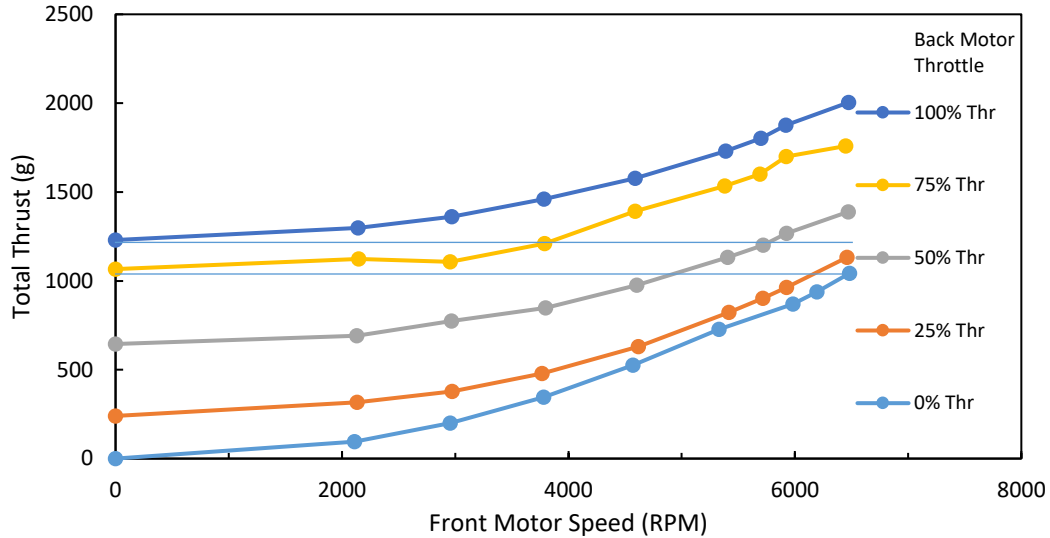


**Figure 27.** The total thrust of the system is the sum of front and back propellers' thrust. The plots seem to have the same form, simply translated vertically.

There is a gap of 190 grams between the rightmost point on the 0% curve and the leftmost point of the 100% curve, as indicated by the thin blue lines running across the graph. Both represent a single motor operating at full throttle. This difference would not exist if the drag on the back, unmoving propeller were not included in the calculation. The single propeller line would reach about 1220 grams, as Figure 25 indicates. Plotting the single rotor curve as the 0% curve would cross the 25% curve and was avoided for consistency of calculations and plots.

Although it is important to note how thrust is affected by motor speeds, it provides only a partial picture of what is occurring. Electric current was measured in power wires to the ESCs for both front and back motors, as shown in Figures 28 and 29, respectively.

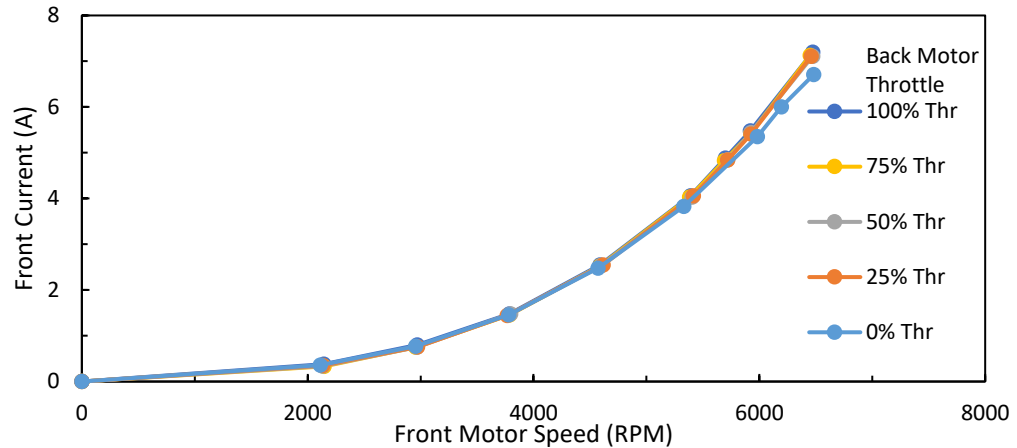


**Figure 28.** The current drawn by the front motor is virtually unaltered by changing back motor throttle settings. A slight reduction occurs when the front propeller's drag induces a spin in the back propeller.

Plots of power consumption, as indicated by the measured quantity of current to the front motor, overlap for the various back motor throttle settings. This suggests complete independence from back motor speed. However, a deviation occurs when the un-driven back propeller is spun by the wake of the front propeller. Current used by the front motor dips below its usual curve. This might be related to a back current induced in the back motor by the spinning magnets of the brushless motor. Alternatively, the back propeller's induced spinning may act as a pressure release and the pressure between the rotors drops enough for the front rotor to more easily propel the air.

Figure 29 plots the back rotor power draw as a measure of current. The form of this plot resembles Figure 26, in which curves that begin level decrease as front motor speed increases. One difference between them is that the positive currents were never negated, as the thrust values were.

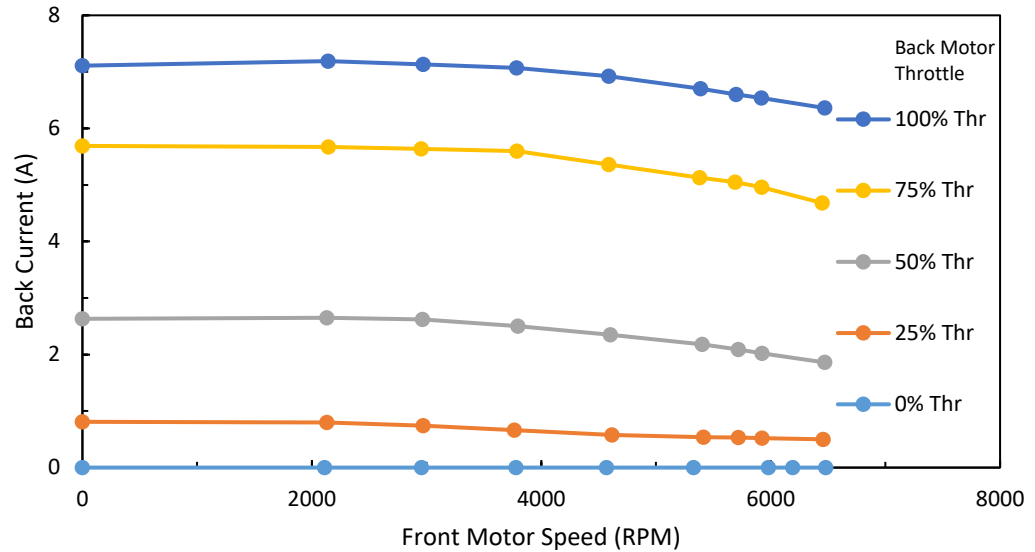


**Figure 29.** The current drawn by the back motor experiences reductions with the increase of the front motor's speed. This reduction in current would not be seen in a biaxial motor arrangement and is a coaxial advantage.

Reductions in current draw are observed for the back motor. This contradicts the presumption that the second motor would have the same power requirements as the first motor. This may be a result of ESC programming. The ESC may sense that the rotor speed matches the desired rotor speed as indicated by the PWM signal. It would then adjust current draw to maintain this rotor speed. Although the lower power use does not seem to be on the same scale as the thrust losses, it signals possible redemption for the coaxial system when performance and efficiency are considered.

In Figure 30, the coaxial pair's power consumption is indicated by electric current. The curves have the same shape regardless of back motor throttle setting but are positioned vertically according to the back motor's initial current draw.

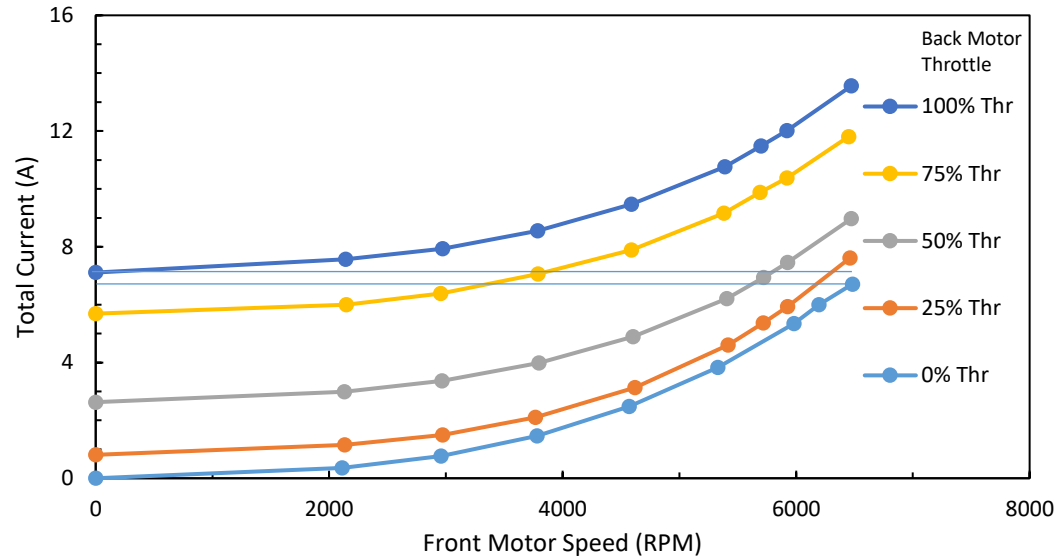


**Figure 30.** The total current drawn by the system is a combination of front and back current draws. The curves are nearly identical curves translated vertically.

The curves for total current strongly resemble the curves for total thrust when both are plotted against the speed of the front motor. There is a gap of 0.4A between the rightmost point on the 0% curve and the leftmost point of the 100% curve, as indicated by the thin blue lines extending across the graph. Both points represent a single motor operating at full throttle. This difference is a result of the deviation in current to the front motor.

The thrust and current of the coaxial pair were plotted against each other in Figure 31. The result is multiple similarly-shaped curves with positive, decreasing slopes. For the most part, the curves overlap, but gaps do exist. These gaps mark places when a specific amount of thrust can be produced for different amounts of power. Alternatively, a certain amount of power could provide different amounts of thrust.

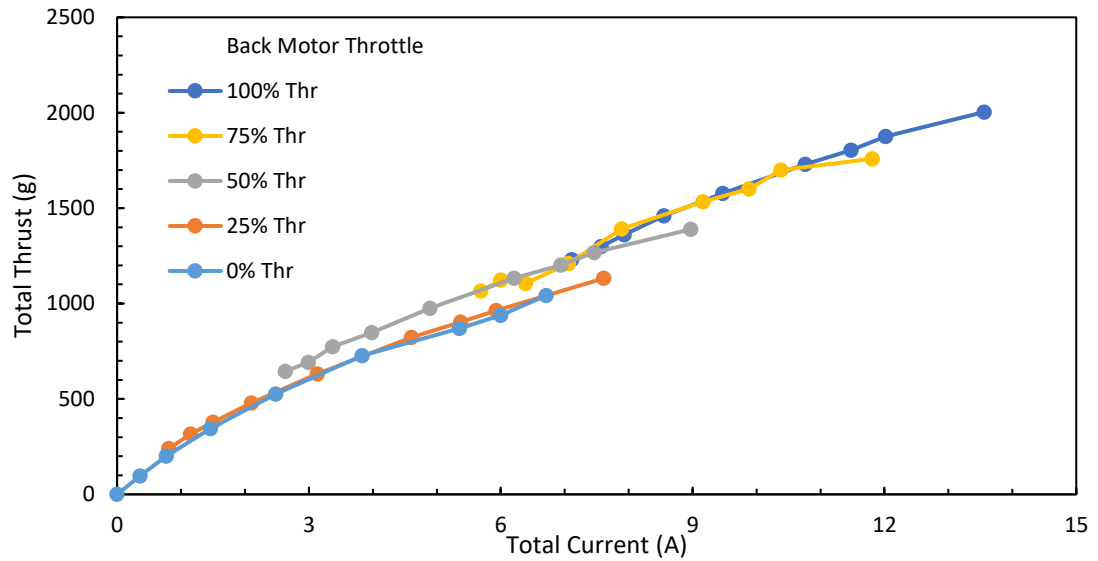


**Figure 31.** Thrust-current curves show opportunities to produce certain amounts of thrust for less current. This indicates that throttle levels can be strategically managed to conserve power with proper mapping.

Opportunities to gain thrust and reduce power usage present themselves and can be exploited. If an autopilot were to be programmed with these data, it could save power and maintain thrust by increasing the back throttle setting and decreasing front throttle setting at certain points.

The mechanical power of the system was calculated as before and divided by the electrical power of the system to yield efficiency values. In Figure 32, system efficiency is used to consider how an autopilot could most efficiently provide thrust to a coaxial multirotor UAV. For a specified thrust, the most efficient operating condition would lie on the uppermost curve.

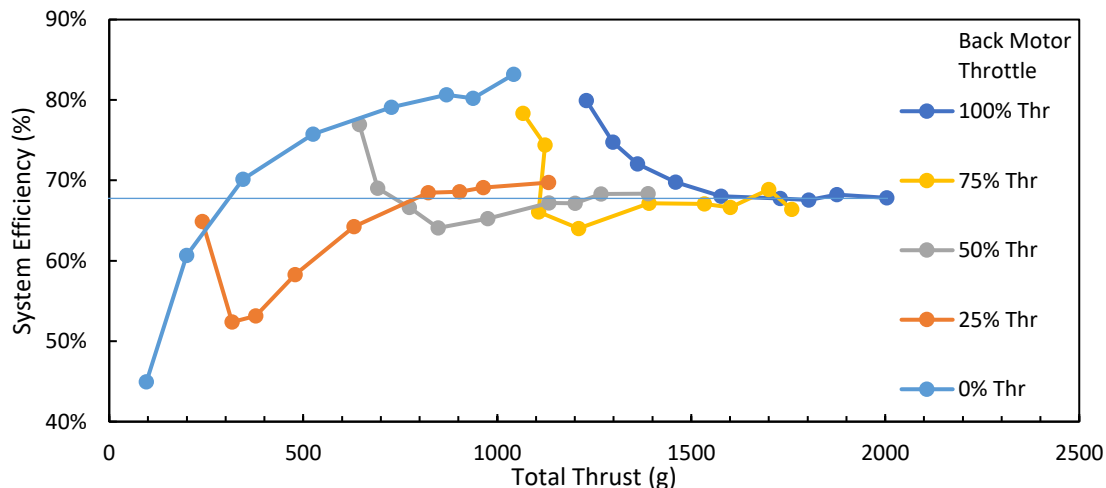


**Figure 32.** The addition of the second motor clearly affects the shape of efficiency curves. Since two curves are above the other plots, they represent the most efficient path to reach maximum thrust: advance one motor to maximum before the other.

According to Figure 32, the single motor represented by the 0% throttle curve will climb to 83% efficiency but two operating motors will consistently converge to approximately 68% efficiency, as indicated by the thin blue line spanning the graph. Since it is usually desirable to manage a system's operation according to efficiency and output, this plot can also be used to strategically adjust throttle settings. The obvious answer is to operate on one motor for as long as possible before the thrust of another propeller is used. This would allow the vehicle to operate at its highest efficiency until it needs more thrust.

To answer the question of which rotor, front or back, operates on its own, thrust values were plotted as a heat map in Figure 33. As front motor throttle increases, the columns are navigated upward. As back motor throttle increases, the rows are navigated rightward. The color gradient represents increasing total thrust from the coaxial rotors. Total thrust is 0 grams when both rotors are off. When they are at their maximum throttle settings, 2000 grams of thrust are produced.

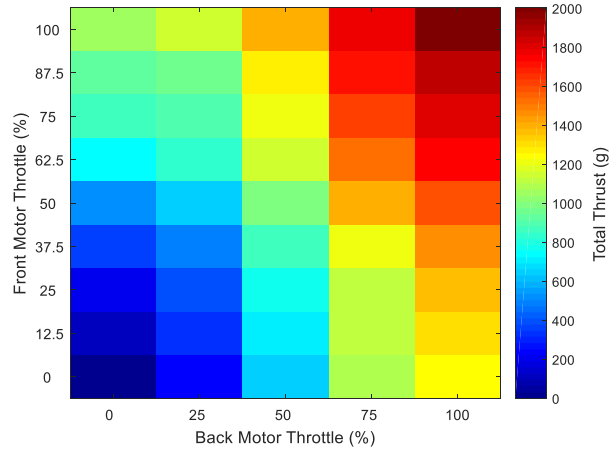


**Figure 33.** A heat map of throttle combinations and thrust shows a steeper gradient when the back motor throttle setting is advanced, as opposed to the front motor throttle setting.

A heat map of the system's total thrust makes it easy to compare the output when different throttle setting combinations are implemented. When only the front throttle is increased, thrust only reaches the green level, about 1000 grams. But when only the back throttle is increased, thrust reaches the yellow level, about 1350 grams. This comparison confirms that it is preferable to have a higher throttle setting on the back motor than on the front motor. With the insights from Figure 32, efficient operation can be accomplished by using the back motor exclusively before implementing the front motor.

This information can be confirmed with the heat map of the system's efficiency, Figure 34. It replaces thrust values from Figure 33 with the corresponding system efficiency values. The darkest zones on the heat map are the throttle settings 50%-100% for either front or back motor. When both rotors are used, efficiency values are in the yellow-orange range, about 68%.

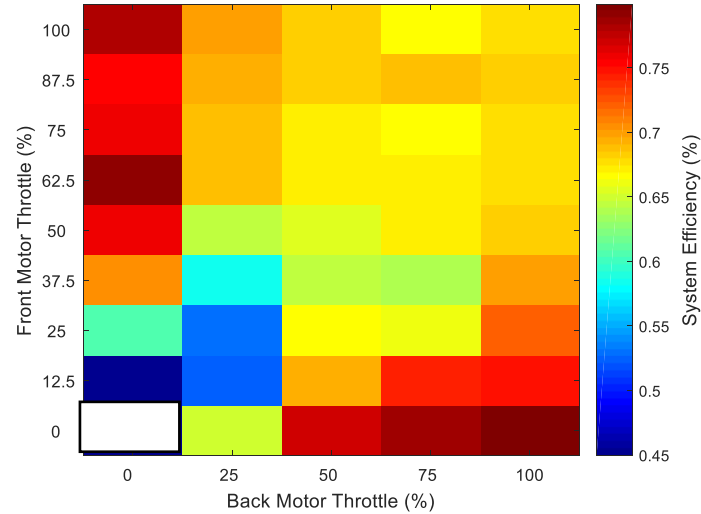


**Figure 34.** A heat map of system efficiency at various coaxial rotor throttle combinations indicates highest efficiency is when the back motor throttle setting is 100%.

Figure 34 shows that it is preferable to have one throttle setting set much higher than the other, essentially operating in the top-left or bottom-right corner. Taken together, the heat maps indicate that both efficiency and thrust are best when back motor throttle is increased to the maximum then front motor throttle is increased to the maximum.

The efficiency of the system is directly related to the performance of the system by way of the motors' speeds. The performance of the system, plotted in Figure 35 below, converges to approximately 6.3 grams of thrust per watt of electricity for the coaxial pair of motors.

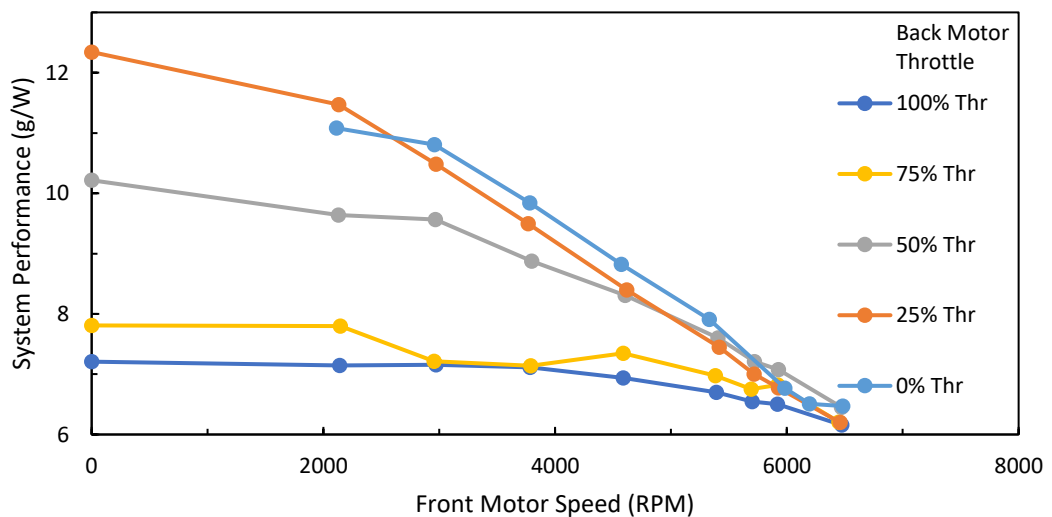


**Figure 35.** Performance decreases as motor speeds increase, converging to about 6.3 g/W for a coaxial pair.

The order of curves in Figure 35 shows that generally, the rotors perform better when the back motor throttle setting is lower. This fits the pattern established in Figure 32 by suggesting the use of one motor exclusively if possible for more efficient operation. The convergence of performance values offers another insight for Figure 32. A single propeller operating at 83% efficiency produces the same thrust for each watt of electricity as a coaxial pair operating at 68% efficiency, but the coaxial pair can produce more thrust.

### 3.3 Two Coaxial Propellers of Different Pitches

As discussed in the Theory section, increasing the pitch of the downstream rotor should be a feasible way to recover lost thrust. A primary concern when studying the effect of propeller pitch is to restrict other propeller differences such as material and design. The best way to do this was to switch from the carbon fiber T-Motors 13"x4.4" propeller to a series of glass fiber composite APC thirteen-inch propellers. Some pitch values were only available for clockwise (left) propellers while others were only available for counterclockwise (right) propellers. When the data were collected using the setup illustrated in Figure 11, they were separated by tests in which propellers spun in the same direction or opposite directions. All data presented are at 100% throttle.

The heat maps in this section are all grids of front propeller pitch and back propeller pitch. Each heat map also includes a color bar that defines the gradient of colors. The bar's label includes the spin direction of the front and back propellers such that LL and RR configurations are co-rotating and LR and RL configurations are contra-rotating. Figure 36, for example, plots the total thrust of co-rotating pairs.

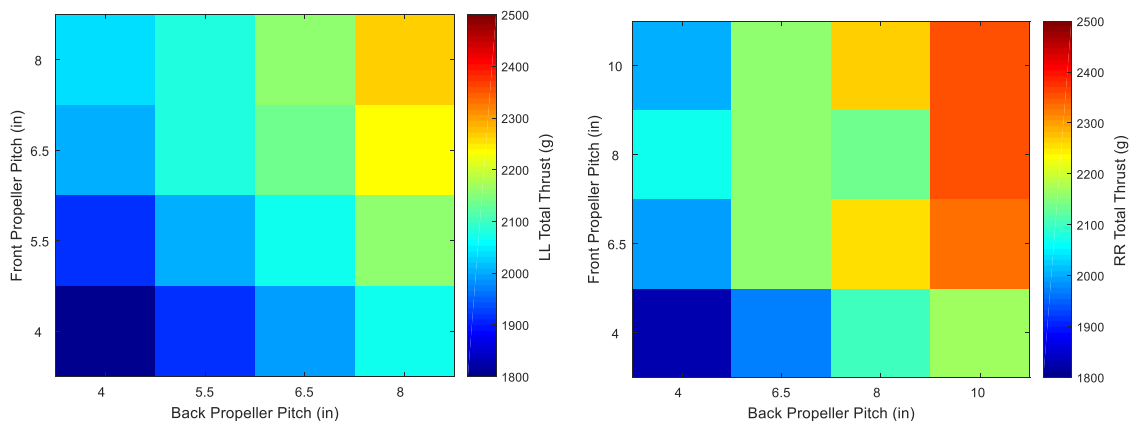


**Figure 36.** Heat maps were made to represent the total thrust of a coaxial pair with the same spin direction. The left map has two clockwise propellers (LL) and the right map has two counter-clockwise propellers (RR).

The above two heat maps show clearly that higher pitches increase total thrust for a propeller pair spinning in the same direction. It is clear from inspection of the LL heat map in Figure 36 that a coaxial system's thrust increases with increasing pitch values. From the heat maps, rows and columns can be compared like in the previous section. Moving right by increasing back propeller pitch increases thrust more effectively than moving up by increasing front propeller pitch.

The heat maps in Figure 37, below, present total thrust values for pairs of contra-rotating coaxial propellers at maximum throttle. They support the conclusion made in the previous paragraph regarding the benefits of higher pitch, especially for the back rotor. The scale indicates that the thrust of a coaxial pair can vary by about 700 grams, depending on the rotors' pitches.

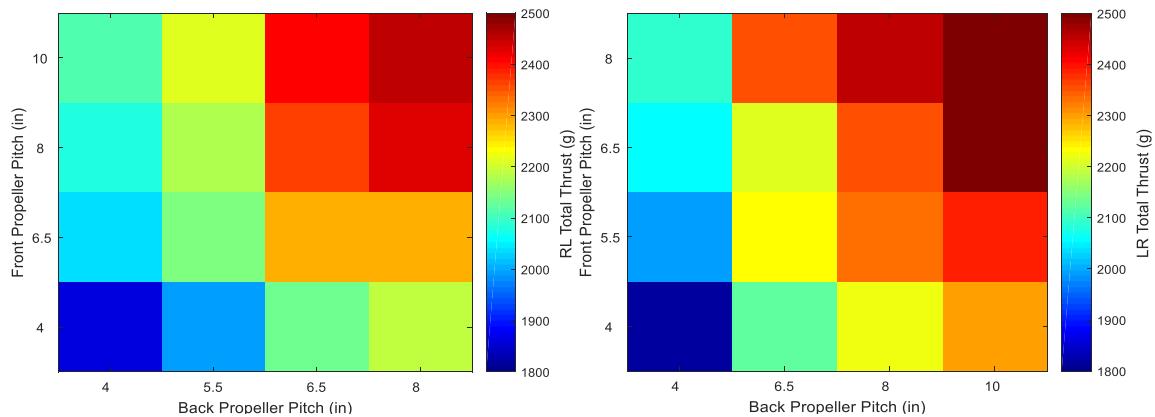


**Figure 37.** Heat maps were made to represent the total thrust of a contra-rotating coaxial pair. The left map has two clockwise propellers (RL) and the right map has two counter-clockwise propellers (LR).

Since the color bars share the same scale, direct comparisons can be made between Figures 36 and 37. The thrust generated by the 10R-10R pair is less than that of the 8L-8R. This suggests that swirl recovery may contribute more to increasing thrust than increasing pitch. The darkest regions amongst these heat maps indicate that the contra-rotating setups have higher thrust output.

Although total thrust is an important property of the system, changing the propellers' pitches was an exercise to compensate for the underperformance of the downstream motor. To bridge the gap between coaxial and multi-axis setups, the back motor and front motor would need to produce thrust in a one-to-one ratio. The ratio of back rotor thrust to front propeller thrust was calculated for all coaxial pairs. For Figures 38 and 39, colors between red and brown indicate that the back rotor's thrust meets or exceeds the thrust generated by the front rotor.

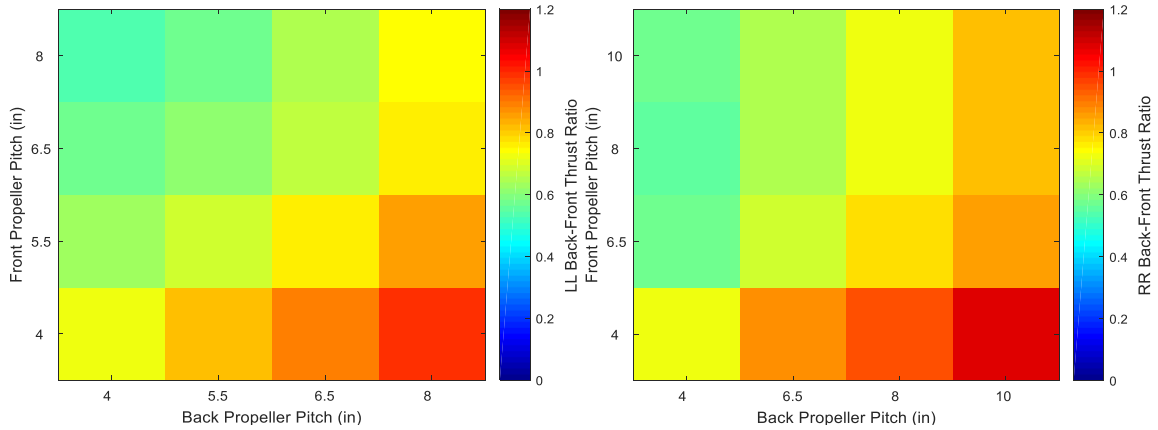


**Figure 38.** Heat maps were made to represent the ratio of the back propeller’s thrust to the front propeller’s thrust. With co-rotating propellers, thrust of a 4-inch pitch propeller is matched by 8-inch or 10-inch pitch.

In pairs with identical spin directions, the ratio of back propeller thrust to front propeller thrust is approximately one when the back propeller’s pitch is at least twice the front propeller’s pitch, as indicated by the reds in the bottom-right corners of the heat maps in Figure 38. This distribution can be achieved by a 4-inch pitch propeller followed by an 8-inch pitch or 10-inch pitch propeller.

For the contra-rotating pairs in Figure 39, the thrust ratio reaches unity slightly sooner. With a 4-inch pitch propeller in front, the system’s thrust can be doubled with a contra-rotating 6.5-inch pitch propeller in the back. For more thrust overall, a 5.5-inch pitch propeller can be followed by a 10-inch pitch propeller to double the system’s thrust. Such a feat is more impressive because the thrust of the 5.5-inch pitch propeller is larger than that of the 4-inch pitch propeller.

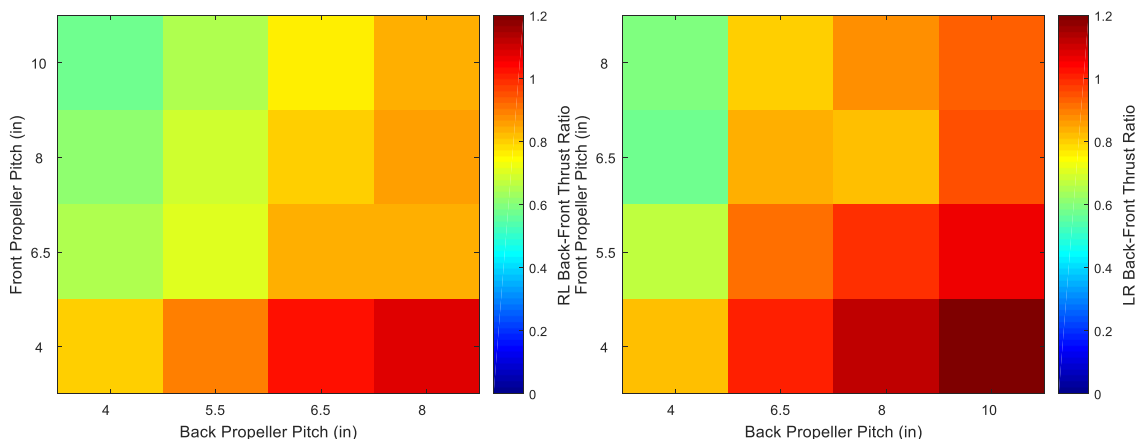


**Figure 39.** Heat maps were made to represent the ratio of the back propeller’s thrust to the front propeller’s thrust. With contra-rotating propellers, thrust of a 5.5-inch pitch propeller is matched by 10-inch pitch.

Having confirmed that coaxial thrust losses are not inevitable, it becomes necessary to extend the lessons of the paired study to a set of four propellers. Propeller choices should be guided based on the metric of performance or efficiency. The heat maps for contra-rotating rotor efficiency found in Figure 40 are not insightful and—instead of providing a clear pattern—provide single hot spots in which front rotor pitch is greater than back rotor pitch. Faster air from a high-pitched front rotor could reduce the current drawn by the back rotor, but that would not explain the high efficiency for the 4R-6.5L combination.

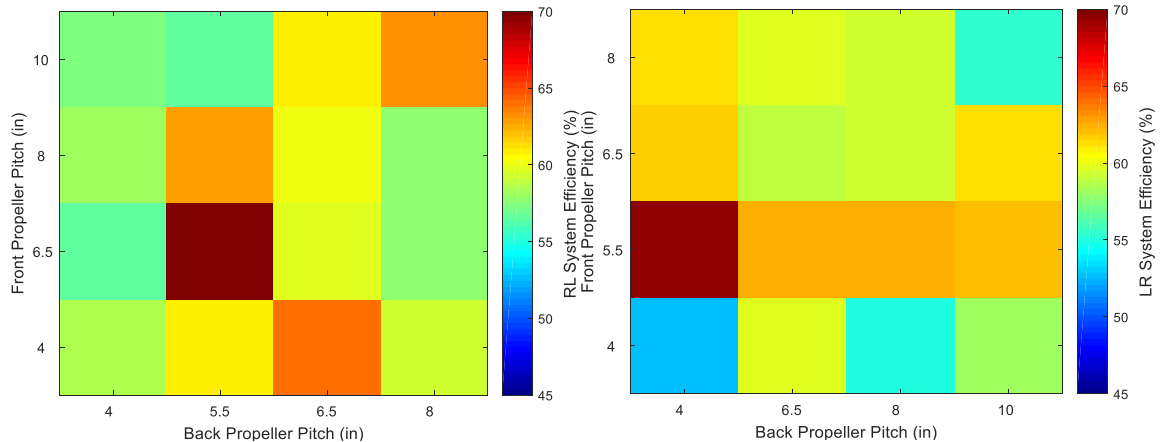


**Figure 40.** System efficiency for contra-rotating pairs are represented as heat maps. They show no clear patterns in increasing efficiency but indicate two high-efficiency pairs, 6.5R-5.5L and 5.5L-4R.

The three darkest zones on the map perform so well that they exceed the estimated performance of a multi-axis setup. Each estimation was the sum of typical thrust values of both propellers when either is the first propeller. In fact, the estimated multi-axis performance values were on average 0.572 grams per watt higher than coaxial performance values, as high as 1.23 grams per watt more and 0.405 grams per watt fewer. In terms of thrust, the multi-axis system was estimated to be on average 282 grams stronger, climbing to 502 grams for a pair of counter-clockwise 8-inch pitch propellers.

Heat maps cannot be marked with error bars per se, but for the pitch-related experiments detailed in the current section and the next section, values of thrust and current were recorded for exactly fifty points. Data collection earlier experiments used closer to two-hundred points. The highest calculated errors for thrust measurements was 10.5 grams and the highest calculated errors for current was 0.45A for any trial.

### 3.4 Four Coaxial Contra-rotating Propellers of Different Pitches

Importantly, the lessons from paired coaxial tests can be extended to four contra-rotating propellers. The above section highlights that increasing propeller pitch downstream yields higher total thrust values.

Figure 39 shows that the thrust of the first propeller can be matched by the second propeller. With this in mind, a system of four propellers should be capable of quadrupling thrust. Six such quadruplets were tested to demonstrate the variability in the system, In Figure 41, the characteristics of the most impressive quadruplet are highlighted. This quadruplet lead with a low-pitch propeller and subsequent propellers had successively higher pitches. Figure 41 enumerates individual rotors' thrust contributions and quantifies each as a percentage of the first rotor's thrust.

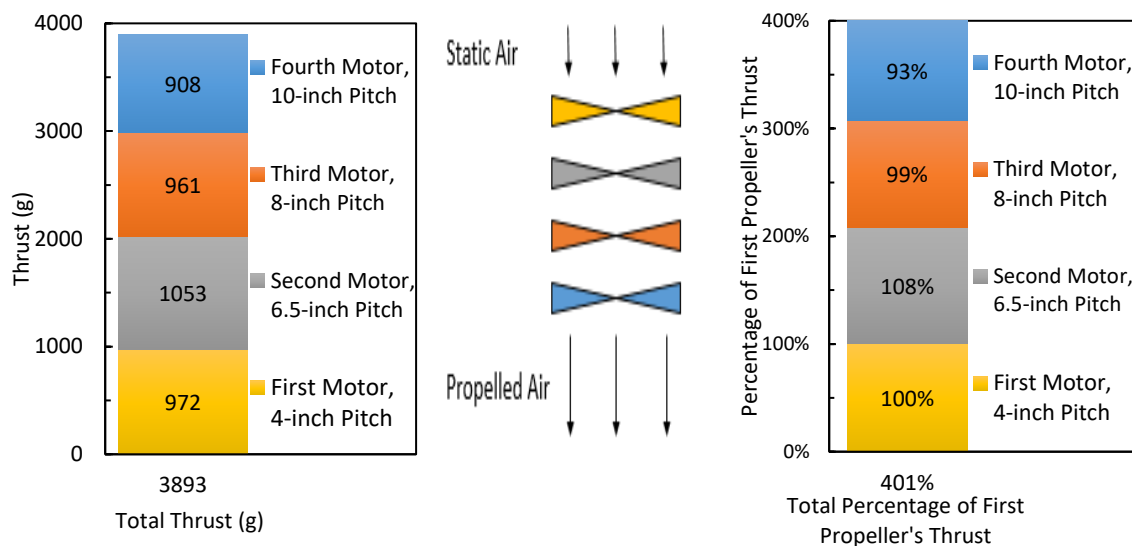


**Figure 41.** Contra-rotating quadruplet (4L-6.5R-8L-10R) proved to be capable of approximately quadrupling the thrust of the 4L propeller.

Varying propeller pitch in each propeller demonstrates the range of thrust, performance, and efficiency values for a four-propeller system. Six orders were chosen to try maximizing or minimizing thrust and maximizing or minimizing efficiency. The most promising combination was 5.5L-6.5R-8L-10R. This order was capable of quadrupling the first propeller's thrust generation because the propeller of lowest pitch was followed by propellers of successively higher pitches. Otherwise, thrust generation may not even triple the thrust of the first rotor. While this quadruplet could reach 401% of the first rotor's thrust at 3893 grams, the 8L-10R-4L-4R combination only produced 266% of its first rotor's thrust at 3286 grams.

In Figure 42, thrust curves for each of the six quadruplets were compared. The curves with highest thrust values have successively increasing pitches. For other propeller combinations, total thrust increased more slowly with respect to current.

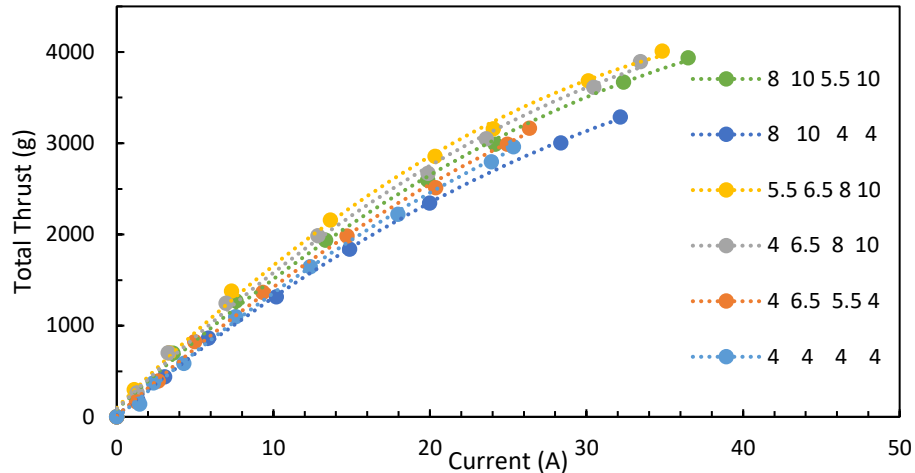


**Figure 42.** Thrust curves for six coaxial quadruplets show the range in total thrust for these systems.

Figure 42 dispels some predictions regarding the relative importance of the first two rotors. , the 4L-4R-4L-4R data have a higher slope than the 8L-10R-4L-4R data but cannot extend as far, suggesting that severely decreasing pitch can render some rotors moot. For high pitch values, higher thrust is expected but in the second case, additional current is expended for simply running the two back motors. When run alone, the 8L-10R combination consumed 21.9A and provided 2530 grams of thrust, which seems to fit comfortably on the trendline. Although a multirotor system could benefit greatly from a coaxial arrangements, some can be an exercise in futility.

The system efficiency of each quadruplet was calculated and plotted against current in Figure 43. Each curve appears to level in efficiency toward higher duty cycles and power usage.

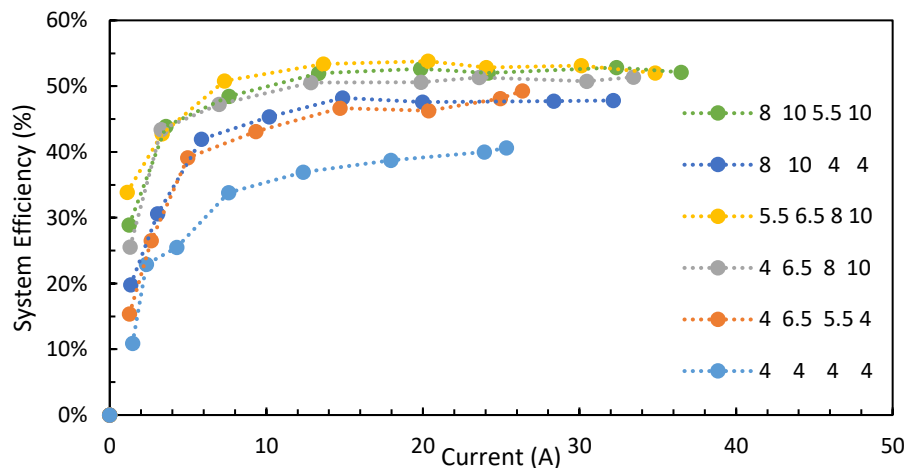


**Figure 43.** Efficiency curves for six coaxial quadruplets show the range for these systems. Generally, systems with higher thrust in Figure 42 have higher efficiencies in this plot.

Reviewing the efficiency of two motor systems with varying pitch provided rare maximum efficiencies about 70%. The four motor systems in Figure 43 reach at most 54% efficiency in the case of 5.5L-6.5R-8L-10R, the champion of thrust production. The least efficient quadruplet is the 4L-4R-4L-4R propeller setup, the second worst thrust producer out of these six combinations, which reaches 40.6%.

In Figure 44, performance curves were plotted to show that the order of the best performing quadruplets is the same order as the most propulsive quadruplets in Figure 42.

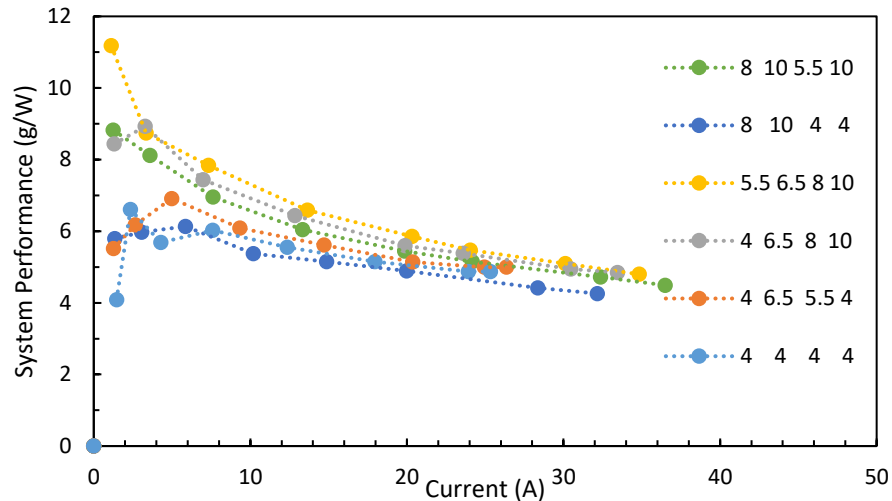


**Figure 44.** Performance curves for six coaxial quadruplets show the range for these systems. Generally, systems with higher thrust in Figure 37 have higher efficiencies in this plot.

The best performing tested set is once again 5.5L-6.5R-8L-10R, ending up providing 4.8 grams of thrust for each watt of electricity. For pairs tested in Section 3.3, the minimum measured performance was about 4.8 grams per watt at full throttle for the 10R-10R rotors.

Another note from Figure 44 is the fact that some plots extend farther right than others. The maximum current values of the curves can be related to the collective pitch of the propellers, which can be defined as the sum (in inches) of the individual propellers. A general trend shows a positive relationship between collective pitch and maximum current in Figure 45.

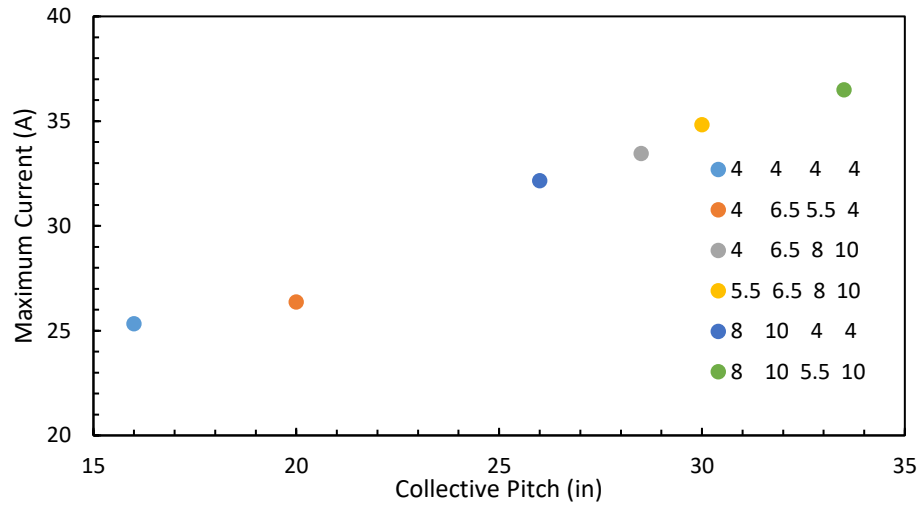


**Figure 45.** The maximum current of the quadruplets is directly related to the collective pitch of the system, the sum of the four propellers' pitch values.

Figure 45 provides a trend that can be supported by data for a coaxial pair, a positive trend exists there as well. However, a given value for collective pitch can be achieved using multiple combinations of propellers and no consideration is given to propeller order. The order and relative pitch of rotors do strongly affect a rotor's thrust generation and current draw because downstream rotors are so heavily affected by their predecessors.

#### 4. Conclusions

The objective of this study was to explore the advantages and disadvantages of coaxial rotors for a multirotor system. Static thrust experiments were done to quantify the losses of a coaxial system with four propellers and examine its behavior when variables such as propeller direction, separation distance, motor speed, and propeller pitch were altered.

Coaxial rotors were tested using up to four propellers with 13-inch diameters. Thrust from downstream propellers were measured with respect to the first propeller. With a pitch of 4.4 inches, contra-rotating second, third, and fourth rotors produced 71%, 53%, and 41% of the first rotor's thrust, respectively. With a pitch of 4.4 inches, co-rotating second, third, and fourth rotors produced 61%, 42%, and 40% of the first rotor's thrust, respectively. This confirmed that contra-rotating coaxial rotors generate more thrust than co-rotating coaxial rotors by effectively recovering the energy put into the swirl of the leading propeller's wake. With a pitch of 10 inches, co-rotating second, third, and fourth rotors produced 97%, 67%, and 54% of the first rotor's thrust, respectively. This demonstrated that downstream propellers are capable of generating more thrust when operating at higher pitches. The thrust losses of the downstream propellers do not have to be as high as they typically are.

Tests varying the distance between the rotors' planes of rotation were also revealing. They showed that although the thrust was still distributed amongst rotors by similar proportions, total thrust generated by the coaxial quadruplets were about 4.5% higher at 2-inch separations as opposed to 8-inch separations.

Varying the relative speeds of a pair of coaxial propellers did not provide any special ratio of front motor speed to back motor speed for improvements in thrust or efficiency. Instead, they demonstrated that a coaxial pair will reach about 68% efficiency, while a single propeller can reach about 83% efficiency. Evidence showed that propulsion would be improved if the downstream propeller were set to spin significantly faster than the upstream propeller. Combining the presented evidence suggested that coaxial multirotor systems should use the downstream rotor exclusively until more thrust is required. At such a point, the downstream rotor will be working at maximum throttle and the upstream rotor's throttle can be adjusted.

The effects of pitch on a coaxial pair were explored as well. Data showed that rotors produced more thrust in total when higher pitches were used and that increasing the pitch of a single rotor is more effective on the downstream rotor. During tests, some combinations of a low-pitch rotor followed by a high-pitch rotor

were able to more than double the thrust produced by the low-pitch rotor alone. In one test, the downstream rotor produced 19% more thrust than the upstream rotor.

Insights from the exploration of pitch effects were extended to the coaxial quadruplets by operating four propellers with varying pitches at separation distances of four inches. In cases where a low-pitch propeller was followed by increasingly higher-pitched propellers, a coaxial quadruplet was able to produce near-equal thrust in each propeller, totaling 401% of the thrust of the first rotor. This served as a strong validation of the work and demonstrating the feasibility of larger coaxial systems.

#### **4.1 Future Experiments**

For these experiments, repetition in a more controlled environment would serve well to validate results. For example, wind tunnel testing can enable dynamic tests wherein the system is operating in a pre-existing flow. In a sufficiently large wind tunnel, the system could be rotated to consider the system's operation in crosswinds.

Additionally, motor speed variation was not applied to coaxial quadruplets in the scope of this study. It is possible that the effects of pitch could be amplified by individually controlling rotor speeds. In flowing air, a vehicle may benefit from operating a low-pitch propeller at higher speeds than high-pitch propellers.

It would also serve well for coaxial systems and the corresponding multi-axis systems to be implemented on test vehicles so that the coaxial may be compared with the ideal setup for thrust generation. During multi-axis comparisons in the study, trends in coaxial thrust and performance were assigned a polynomial fit. From this, information was extrapolated about six- and seven-propeller coaxial setups. Experimental evaluation might reveal possible limits for coaxial rotors.

The inter-rotor separation distance of a coaxial system should be studied further. Smaller distances could be used to determine at what point two two-bladed propellers might begin behaving like a single four-bladed propeller.

### References

1. Wang, Q., "The Current Research Status and Prospect of Multi-rotor UAV," *Journal of Mechanical and Civil Engineering*, Vol.14, No.4, 2017, pp.31-35.
2. Otsuka, H. and Nagatani, K., "Thrust Loss Saving Design of Overlapping Rotor Arrangement on Small Multirotor Unmanned Aerial Vehicles," *IEEE International Conference on Robotics and Automation (ICRA)*, 2016, pp. 3243-3248.
3. Barr, J. M. and Wilson, A. M., "A Feasibility Study of Using Unmanned Aerial Vehicles to Survey Avian Abundance by Using Audio Recording," Elizabethtown College, PA, 2015.
4. Pandit, V. and Poojari, A., "A Study on Amazon Prime Air for Feasibility and Profitability—A Graphical Data Analysis," *Journal of Business and Management*, Vol. 16, No. 11, 2014, pp. 6-11.
5. "European Drones Outlook Study," SESAR Joint Undertaking, 2016.
6. Coleman, C. P., "A Survey of Theoretical and Experimental Coaxial Rotor Aerodynamic Research," NASA Technical Paper 3675, 1997.
7. Taylor, M. K., "A Balsa-Dust Technique for Air0Flow Visualization and its Application to Flow through Model Helicopter Rotors in Static Thrust," NACA TN 2220, 1950.
8. Zimmer, H., "The Aerodynamic Calculation of Counter Rotating Coaxial Rotors," *Eleventh European Rotorcraft Forum*, Paper No. 27, The City University, London, 1985.
9. Min, K., Chang, B., and Seo, H., "Study on the Contra-Rotating Propeller system design and full-scale performance prediction method," *International Journal of Naval Architecture and Ocean Engineering*, Vol. 1, No. 1, pp.29-38, 2009.
10. Leishman, J. G., and Ananthan, S., "Aerodynamic Optimization of a Coaxial Propeller," 62<sup>nd</sup> Annual Forum and Technology Display of the American Helicopter Society International, Phoenix, AZ, 2006.
11. Rand, O. and Khromov, V., "Aerodynamic Optimization of Coaxial Rotor in Hover and Axial Flight," 27<sup>th</sup> International Congress of the Aeronautical Sciences, 2010.
12. Yana, J. and Rand, O., "Performance Analysis of a Coaxial Rotor System in Hover: Three Points of View," 28<sup>th</sup> International Congress of the Aeronautical Sciences, 2012.
13. Xu, H. and Ye, Z., "Numerical Simulation of Unsteady Flow Around Forward Flight Helicopter with Coaxial Rotors," *Chinese Journal of Aeronautics*, Vol. 24, No. 1, pp. 1-7, 2011.

14. Wachspress, D. A. and Quackenbush, T. R., "Impact of Rotor Design on Coaxial Rotor Performance, Wake Geometry and Noise," American Helicopter Society 62<sup>nd</sup> Annual Forum, Phoenix, AZ, 2006.
15. Kim, H. W., Duraisamy, K., and Brown, R., "Aeroacoustics of a Coaxial Rotor in Level Flight," American Helicopter Society 64<sup>th</sup> Annual Forum, Montreal, QC, 2008.
16. Zhu, Z., Zhao, Q. and Li, P., "Unsteady flow interaction mechanism of coaxial rigid rotors in hover," *Acta Aeronautica et Astronautica Sinica*, Vol. 37, No. 2, pp.568-578, 2016.
17. Barbely, N. L., Komerath, N. M. and Novak, L. A., "A Study of Coaxial Rotor Performance and Flow Field Characteristics," 2016 AHS Technical Meeting on Aeromechanics Design for Vertical Lift, San Francisco, CA, 2016.
18. Lim, J. W., McAlister, K. W. and Johnson, W., "Hover Performance Correlation for Full-Scale and Model-Scale Coaxial Rotors," American Helicopter Society 63<sup>rd</sup> Annual Forum, Virginia Beach, VA, 2007.
19. Brandt, J. B. and Selig, M. S., "Propeller Performance Data at Low Reynolds Numbers," 49<sup>th</sup> AIAA Aerospace Sciences Meeting, AIAA 2011-1255 Orlando, FL, 2011.
20. Merchant, M. P., "Propeller Performance Measurement for Low Reynolds Number Unmanned Aerial Vehicle Applications," Master's Thesis, College of Engineering, Wichita State Univ., Wichita, KS, 2005.
21. Intaratep, N., Alexander, W. N., Devenport, W. J., Grace, S. M. and Dropkin, A., "Experimental Study of Quadcopter Acoustics and Performance at Static Thrust Conditions," 22<sup>nd</sup> AIAA/CEAS Aeroacoustics Conference, AIAA 2016-2873, Lyon, France, 2016.
22. Yoon, S., Lee, H. C. and Pulliam, T. H., "Computational Analysis of Multi-Rotor Flows," AIAA SciTech, San Diego, CA, 2016.
23. Aleksandrov, D. and Penkov, I., "Optimal Gap Distance Between Rotors of Mini Quadrotor Helicopter," 8<sup>th</sup> International DAAAM Baltic Conference, Tallinn, Estonia, 2012.
24. Shahmiri, F., "Experimental Investigation of the Hovering Performance of a Twin-Rotor Test Model," *Journal of Aerospace Science and Technology*, Vol. 10, No. 2, pp.1-7, 2013.
25. Shahmiri, F., "Twin-rotor hover performance examination using overlap tests," *Aircraft Engineering and Aerospace Technology*, Vol. 89, No. 1, pp. 155-163, 2017.

26. Theys, B., Dimitriadis, G., Hendrick, P. and De Schutter, J., "Influence of propeller configuration on propulsion system efficiency of multi-rotor Unmanned Aerial Vehicles," International Conference on Unmanned Aircraft Systems (ICUAS), Arlington, VA, 2016.
27. Brazinskas, M., Prior, S. D. and Scanlan, J. P., "An Empirical Study of Overlapping Rotor Interference for a Small Unmanned Aircraft Propulsion System," *Aerospace*, MDPI, Basel, Switzerland, 2016.
28. Prior, S. D., Karamanoglu, M., Odedra, S., Erbil, M. A. And Foran, T., „Development of a Co-Axial Tri-Rotor UAV," 24<sup>th</sup> International UAV Systems Conference, Bristol, UK, 2009.
29. Prior, S. D. and Bell, J. C., "Empirical Measurements of Small Unmanned Aerial Vehicle Co-Axial Rotor Systems," *Journal of Science and Innovation*, Vol. 1, No. 1, pp. 1-8, 2011.
30. Lee, T. E., "Design and Performance of a Ducted Coaxial Rotor in Hover and Forward Flight," Master's Thesis, Dept. of Aerospace Engineering, Univ. of Maryland, College Park, MD, 2010.
31. Geldenhuys, H. J., "Aerodynamic Development of a Contra-Rotating Shrouded Rotor System for a UAV," Master's Thesis, Dept. of Mechanical and Mechatronic Engineering, Stellenbosch Univ., Matieland, South Africa, 2015.
32. Leishman, J. G., *Principles of Helicopter Aerodynamics*, Cambridge University Press, 2006, pp. 55-114.